

Scuola di Scienze  
Dipartimento di Fisica e Astronomia  
Corso di Laurea in Fisica

**Sensitivity and uncertainty analyses on  
ZED-2 reactor criticality calculations  
with ENDF/B-VII.1 and recently  
measured  $^{155,157}\text{Gd}(n,\gamma)$  cross-sections at  
n\_TOF - CERN**

**Relatore:**  
Prof. Cristian Massimi

**Presentata da:**  
Ruggero Rosselli

**Correlatore:**  
Dott. Patrizio Console Camprini

# Abstract

I veleni bruciabili sono una categoria di isotopi impiegata come dispositivo di sicurezza nei moderni reattori nucleari. Gli isotopi dispari del gadolinio  $^{155}\text{Gd}$  e  $^{157}\text{Gd}$  sono potenti veleni bruciabili, largamente impiegati in reattori di potenza di seconda e terza generazione. Le sezioni d'urto degli isotopi  $^{155,157}\text{Gd}$  sono state misurate più volte in passato, ma sembra esserci ulteriore margine di miglioramento. Inoltre, una conoscenza precisa delle sezioni d'urto dei due isotopi è richiesta per ragioni di sicurezza. Nel 2016, in risposta alla necessità di dati migliori, le sezioni d'urto di  $^{155,157}\text{Gd}$  sono state misurate presso la struttura n\_TOF, CERN. L'obiettivo di questa tesi è calcolare un benchmark scelto, in modo da valutare l'impatto delle nuove sezioni d'urto del gadolinio. Inizialmente, vengono introdotti i metodi computazionali per affrontare il problema di benchmark. Successivamente, il reattore di ricerca canadese ZED-2 viene scelto come caso studio per calcoli di criticità attraverso il codice MCNP6.2, eseguito sui sistemi CRESCO (ENEA). Le simulazioni mostrano che il reattore ZED-2 è sensibile a variazioni delle sezioni d'urto del gadolinio. L'impatto dei dati di sezioni d'urto del gadolinio della libreria ENDF/B-VII.1 è valutato attraverso quattro modelli di benchmark, ognuno con diversa concentrazione di gadolinio. È presente un bias di  $-45 \pm 7$  pcm/ppm Gd del valore di reattività al variare della concentrazione di gadolinio, considerando dati dalla libreria ENDF/B-VII.1. I medesimi benchmark sono valutati rispetto ai nuovi dati del gadolinio di n\_TOF, mantenendo il resto del problema invariato. In questo caso, è presente un bias minore di  $19 \pm 6$  pcm/ppm Gd. I nuovi dati sembrano correggere parzialmente le discrepanze tra risultati calcolati e sperimentali, nel contesto di benchmark del reattore ZED-2 con codice MCNP.

# Abstract

Burnable reactor poisons are a class of isotopes used as safety devices in modern power reactor cores. Gadolinium odd isotopes  $^{155}\text{Gd}$  and  $^{157}\text{Gd}$  are powerful burnable poisons, heavily employed in GEN-II and GEN-III power reactors. The  $^{155,157}\text{Gd}$  cross-sections have been measured in the past, and indications are that there is still room for improvement. Additionally, accurate knowledge of the isotopes cross-sections is required for safety reasons. In 2016, to answer the need of improved data,  $^{155,157}\text{Gd}$  cross-sections were measured at the n\_TOF facility, CERN. The goal of this work is to evaluate a selected benchmarking problem, in order to assess the impact of the new gadolinium cross-sections data. Initially, the computational methods necessary to evaluate the benchmark are introduced. The Canadian ZED-2 research reactor is then chosen as a case study in order to compute criticality calculations via the MCNP6.2 code, run on CRESCO systems (ENEA). The ZED-2 reactor is shown to be sensitive to gadolinium cross-sections data variations. The impact of gadolinium cross-section data from the ENDF/B-VII.1 library on the reactivity worth values is assessed through four reactor benchmark models, each with different gadolinium concentration. A bias of  $-45 \pm 7$  pcm/ppm Gd in the reactivity worth with respect to gadolinium concentration is present with data from the ENDF/B-VII.1 library. The same benchmarks are evaluated with respect to the new n\_TOF gadolinium data, maintaining the rest of the problem unaltered. In this case, a smaller bias of  $19 \pm 6$  pcm/ppm Gd is present. The new data seems to partly correct the discrepancies between calculated and experimental values, in the context of MCNP code ZED-2 reactor benchmarks.

# Contents

<b>Introduction</b>	<b>5</b>
<b>1 Gadolinium Cross Sections</b>	<b>8</b>
1.1 $^{155,157}\text{Gd}(n,\gamma)$ cross-sections evaluations and scientific reasons for reassessment . . . . .	8
1.2 n_TOF campaign for Gd cross-sections measurements . . . . .	9
1.2.1 The n_TOF facility . . . . .	10
1.2.2 Experimental setup and Data analysis . . . . .	11
<b>2 Computational Methods</b>	<b>13</b>
2.1 The eigenvalue problem . . . . .	13
2.1.1 Power Iteration . . . . .	15
2.1.2 Convergence assessment . . . . .	16
2.2 Sensitivity and uncertainty analysis . . . . .	18
2.3 MCNP code . . . . .	19
2.3.1 Criticality calculations . . . . .	20
2.3.2 Tallies . . . . .	21
<b>3 ZED-2 Reactor Benchmarks</b>	<b>22</b>
3.1 The ZED-2 reactor . . . . .	22
3.2 Benchmark calculations . . . . .	23
3.3 Reactor configurations . . . . .	28
3.3.1 Model calibration . . . . .	29
3.4 ENDF/B-VII.1 results and data analysis . . . . .	30
3.4.1 Convergence . . . . .	30
3.4.2 Neutron Spectra . . . . .	31
3.4.3 Sensitivity analysis . . . . .	32
3.5 ENDF/B-VII.1 and n_TOF data comparison . . . . .	35
3.5.1 $k_{eff}$ Uncertainties . . . . .	35
<b>Conclusion</b>	<b>37</b>
<b>A Acronyms and Abbreviations</b>	<b>40</b>

# Introduction

In 1939, physicists Leó Szilárd and Albert Einstein sent a letter to the United States President Franklin D. Roosevelt warning that progress in nuclear science had been made to the point where it was possible to develop powerful, atom-powered bombs. Soon thereafter, the Manhattan Project began in the United States, together with worldwide research in Nuclear Science and Engineering. Fortunately, nuclear fission was not only used to build the well-known mass destruction weapons, but also for the benefit of mankind, through the development of uranium-fuelled power reactors.

In modern times, international organisations regulate and supervise the access to nuclear technologies, assisting member states with their peaceful use. The most important international organisation is the IAEA (International Atomic Energy Agency [1]), which counts 172 member states. The IAEA promotes nuclear safety and sets the security standards in the use of nuclear technology and materials, including but not limited to the energy sector. In fact, their mission is “to secure or provide materials, services, equipment and facilities” as well as “to foster exchange of scientific and technical information and training”. It represents the most important Agency in the nuclear technology field.

On the other hand, the CTBTO (Comprehensive Nuclear-Test-Ban Treaty Organization) focuses specifically on preserving the peaceful use of nuclear materials and technologies, while formally banning all nuclear explosions worldwide and detecting and reporting any illegal test.

In the energy sector, a lot of efforts and resources are dedicated to the study of nuclear safety, with the aim of introducing always enhanced standards. The present work, then, ascribes to the field of nuclear safety studies, with focus on a particular class of isotopes used in modern power reactors.

## Nuclear Reactors

Let us initially describe behavioural aspects of a usual nuclear reactor core. There are four classes of materials present in the core: the fuel, the moderator, neutron absorbers and structural materials.

The fuel is of course the source of the thermal energy. For instance, when a neutron fissions a  $^{235}\text{U}$  atom, energy is released in the form of heat together with additional neutrons. But the chain reaction would not self-sustain unless very specific conditions are kept in the reactor core. To achieve the required *neutron spectrum* (the neutron distribution in energy), moderators are employed. Moderating isotopes are generally light particles, which neutrons can scatter on in order to slow down

from fast fission energy. For example, reactors which use natural uranium are known as *heavy water* moderated reactors. Here, the water molecules contain deuterium instead of hydrogen, which is much more efficient in slowing down the neutrons.

A different role is played by the isotopes known as neutron absorbers, or *poisons*. Whereas moderators serve only to slow down the neutrons from fast to thermal energies, poisons *absorb* the neutrons, hence “removing” them from the fission spectrum and inhibiting the chain reaction. Finally, we may classify as “structural materials” all of the remaining materials in the reactor core, whose effects on the reactor neutronics vary from isotope to isotope. In general, structural materials do not contribute to the neutron multiplication and, in fact, absorb a part of the neutron flux. It is also worth mentioning that these materials activate during the life of the core and are a major source of radioactivity, even after shutdown.

The reactor poisons introduced above can be of different kinds and originate from different sources. They can be fission products, like the isotopes of the elements xenon and samarium. Xenon, for example, is a powerful poison which builds up after reactor shutdown and entails a period of inactivity before the reactor can be operative again. However, neutron absorbers can also feature in reactor cores as safety devices. For example, they might be employed in the form of fixed or removable rods inserted in the core or artificially injected into the moderator in the form of soluble compounds.

The classes of isotopes mentioned above determine the behaviour of the reactor core. It is useful to describe the reactor core in terms of its *reactivity*, which is a measure of the stability of the reactor and is related to the effective multiplication factor (see Chapter 2). The reactivity worth is then defined as the amount of additional (positive or negative) reactivity yielded when some external factor affects the reactor core. For example, some reactors can be operated by moving so-called control rods, upwards or downwards with respect to the core. For example, the extraction of a poisoning control rod determines the addition of a positive reactivity worth. Conversely, the reactivity worth of a poison injection into the core will be negative.

In this work, the focus will be on a particular class of poisoning isotopes, namely burnable reactor poisons.

## Burnable Reactor Poisons

Burnable poisons are a class of isotopes widely used in modern reactor cores to limit excess reactivity and mitigate localised power peaking [2]. Reactor poisons are competitors to the fuel isotopes, as they have thermal absorption cross-sections comparable to the fuel fission cross-section. In other words, by absorbing thermal neutrons, which would otherwise cause fission, poisons inhibit the neutron chain reaction.

Natural gadolinium is widely used as a burnable reactor poison in LWRs (light water reactors) [3], for example in the form of gadolinia (gadolinium oxide  $Gd_2O_3$ ) inside the fuel matrix. The use of gadolinium in fuel assemblies allows for higher initial fuel enrichment, which would otherwise be forbidden for safety reasons. The moderation of the reactivity at the BOL (beginning of life) then ensures longer fuel

cycles. As it is shown in Fig. 1, the presence of burnable poisons like boron means that at some point in time a reactivity maximum occurs.

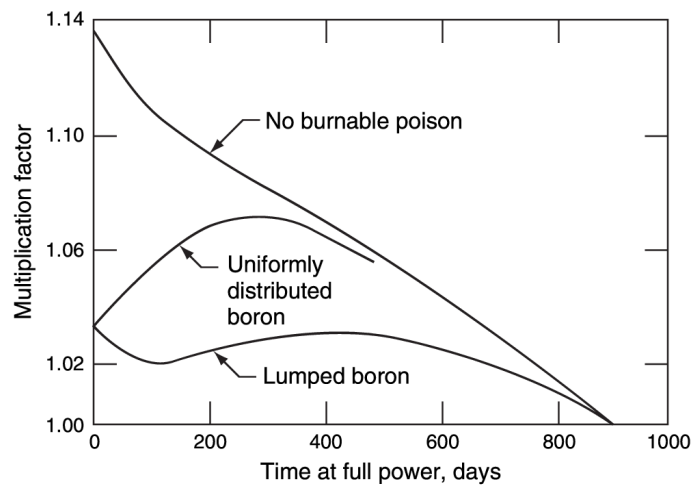


Figure 1: Multiplication factor as a function of time in three different cases, from E. E. Lewis, *Fundamentals of Nuclear Reactor Physics* [2].

Accurate knowledge of neutron poisons - such as gadolinium - absorption cross-sections is therefore required in order to predict when the peak will occur and how intense it will be. Both of these two factors (timing and intensity of the peak) are relevant for the assessment of criticality safety margins in SFPs (spent fuel pools).

Gadolinium is also used in CANDU (Canada Deuterium Uranium) heavy water reactors. In this case, gadolinium nitrate is injected into the heavy water moderator in case of reactivity excursions. Again, for safety reasons, precise knowledge of Gd absorption cross-sections is desired.

In this work we will then outline the differences between different sets of gadolinium cross-sections data present in the literature. Reasons will be given for the need of more accurate data. At the same time, we will evaluate benchmarks for the Canadian ZED-2 research reactor and calculate the effective multiplication factor's ( $k_{eff}$ ) sensitivity to  $^{155,157}\text{Gd}(n,\gamma)$  cross-sections. Finally, we will assess the impact of the data measured by the n\_TOF collaboration at the European Council for Nuclear Research (CERN), in the context of ZED-2 reactor criticality calculations.

# Gadolinium Cross Sections

In this chapter, the gadolinium cross-sections evaluations are analysed and the differences between different sets of data are outlined. Scientific reasons for the re-assessment of the gadolinium odd isotopes cross-sections are given. In conclusion, the main results of the 2016 measurement campaign carried out at n\_TOF (CERN) are discussed and compared to the previous evaluations.

## 1.1 $^{155,157}\text{Gd}(n,\gamma)$ cross-sections evaluations and scientific reasons for reassessment

Most commercial nuclear reactors are thermal-nuclear reactors, i.e. the reactor core is operated with a thermal neutron spectrum. In these kind of reactors, fission occurs via thermal neutrons, conventionally taken with energy  $E = k_B T = 0.0253$  eV, where  $T = 293.61$  K is the room temperature [4] and  $k_B$  is the Boltzmann constant. In the non-relativistic approximation, the speed of a thermal-energy neutron is determined as  $v = \sqrt{2E/m} = 2200$  m/s. The thermal regime is the energy range where neutrons are most likely to fission the fuel atoms, i.e. where the fuel's fission cross-section is higher. Gadolinium is then chosen as a burnable reactor poison because of the high thermal absorption cross-sections of two of its odd isotopes,  $^{157}\text{Gd}$  (15.65% abundance) and, to a lesser extent,  $^{155}\text{Gd}$  (14.80% abundance).

$^{155,157}\text{Gd}(n,\gamma)$  cross-sections have been measured a few times in the past decades, but unfortunately, the reported results are not consistent with one another. In 2006, for example, Leinweber et al. [5] reported a  $^{157}\text{Gd}(n,\gamma)$  thermal cross-section of 226 kb, which is 11% smaller than the ENDF/B-VII.1<sup>1</sup> evaluation of around 254 kb (Mughabghab [7], 2006).

In addition, nuclear reactor experiments and simulations have shown discrepancies between calculated and experimental reactor parameters. An article published in 2016 by Bernard and Santamarina [8] showed that while the data (from the JEFF-3.1.1 library<sup>2</sup>) allows for overall correct predictions of isotopics burnup in the EPR<sup>TM</sup> GEN-III reactor (European Pressurised Reactor), still some C/E (calculated/experimental) biases are found for strong absorbers data.

---

<sup>1</sup>The ENDF/B file is the Evaluated Nuclear Data File produced by the collaboration between the United States and Canada, compiled in the standard ENDF format [6].

<sup>2</sup>The JEFF file is the Joint Evaluated Fission and Fusion file, produced by the OECD-NEA.

The experiment led by Bernard and Santamarina was a simulation of the Gedeon-II campaign, carried out from 1985 to 1988 in Grenoble. The experiment consisted of irradiation and post-irradiation examinations of the PWR (pressurised water reactor) FAs (fuel assemblies). In particular, the Bernard and Santamarina simulation demonstrated how the depletion of  $^{155}\text{Gd}$  and  $^{157}\text{Gd}$  (with cross-sections from the JEFF-3.1.1 library) is slightly underestimated, probably indicating that Gd nuclear data is incorrect (at least in the irradiation energy range).

It is also worth to mention the work from van der Marck [9] (2012), which contains the evaluations of more than 2,000 benchmarks from the ICSBEP (International Criticality Safety Benchmark Evaluation Project [10]) via MCNP code simulations, with data from different nuclear data libraries. Out of the total number of evaluated benchmarks, 164 are no burnup, zero-power calculations containing gadolinium. Among the results of these simulations, there are some non-negligible discrepancies in the C/E ratios and it can be found that a bias is present, ranging from around -578 pcm in the case of the JEFF-3.1.1 library to around -500 pcm for the JENDL-4.0 library. The meaning of “bias” here is that there is a constant underestimation or overestimation of some quantity (for example, calculated and experimental reaction rates). Therefore, it is again indicated that the Gd cross-sections data are to an extent incorrect.

In 2012, experiments were conducted at the ZED-2 facility, AECL, Canada, addressing the discrepancies in the Leinweber et al. [5] data. A full treatment of the ZED-2 research reactor will be given in the third chapter as a case study, where our own MCNP benchmark simulations are analysed. A more detailed summary of different  $^{155,157}\text{Gd}(n,\gamma)$  cross-sections evaluations and reasons for reassessment can be found in Rocchi et al. [3].

Figures 1.1 and 1.2 are plots of the main  $^{157}\text{Gd}$  isotope cross-sections evaluations available on the OECD-NEA (Nuclear Energy Agency) database, plotted with the JANIS [11] software.

## 1.2 n\_TOF campaign for Gd cross-sections measurements

In light of indications of allegedly incorrect Gd cross-sections data, in 2015 an international collaboration began, involving national and international organisations such as the Italian INFN (National Institute for Nuclear Physics), ENEA (Italian National Agency for New Technologies, Energy and Sustainable Economic Development), Geneva’s CERN (European Organisation for Nuclear Research) and the University of Bologna, in order to carry out experiments and obtain new cross-section data for Gd odd isotopes  $^{155}\text{Gd}$  and  $^{157}\text{Gd}$ . In 2016, 4 high-purity Gd samples were acquired from ORNL (Oak Ridge National Laboratories) and beam time was allocated at the n\_TOF (CERN) facility. The experimental campaign and the obtained results will now be briefly described.

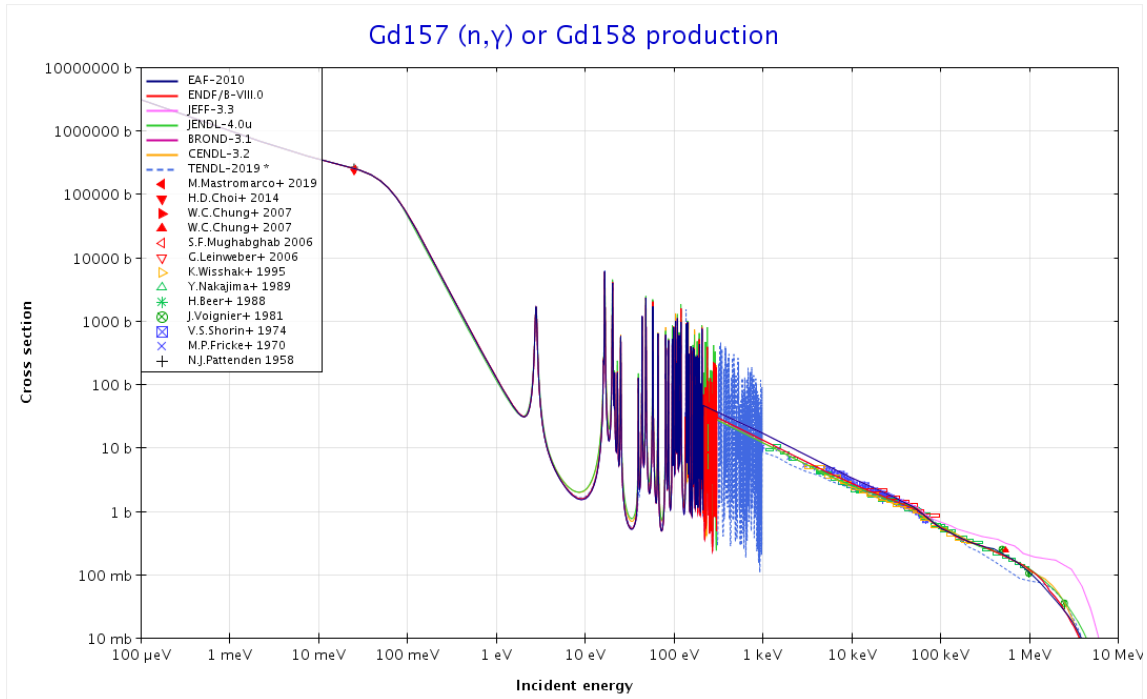


Figure 1.1: JANIS [11] plot of  $^{157}\text{Gd}(n,\gamma)$  cross-sections from a collection of different libraries, plotted from  $10\ \mu\text{eV}$  to  $100\ \text{MeV}$ .

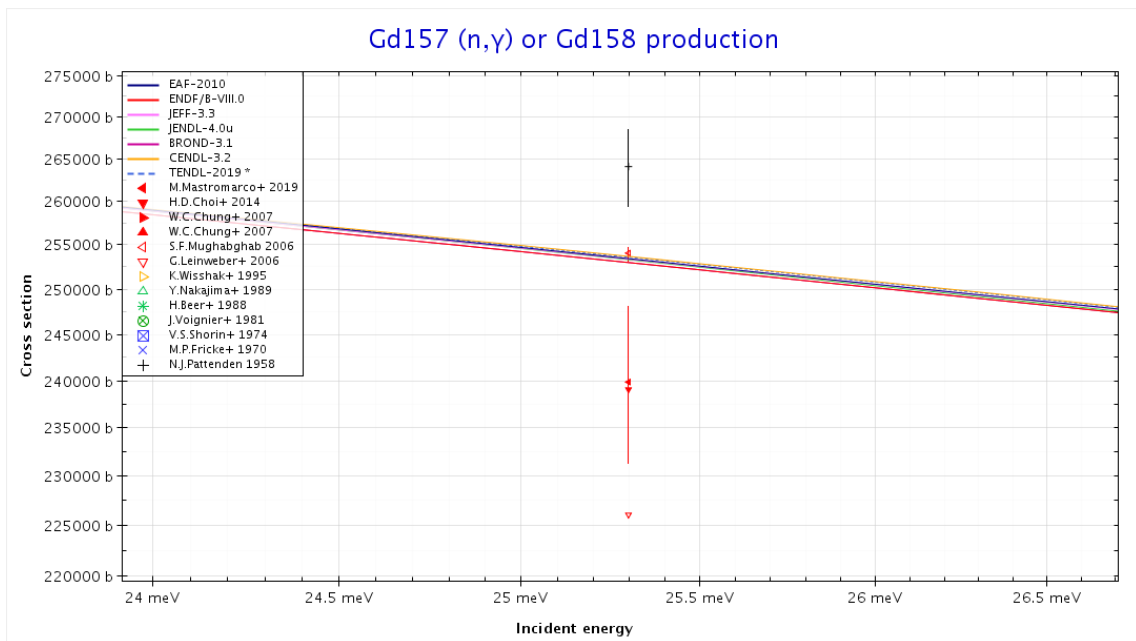


Figure 1.2: JANIS [11] plot of  $^{157}\text{Gd}(n,\gamma)$  cross-sections from a collection of different libraries, plotted about the  $E = 0.0253\ \text{eV}$  thermal point.

### 1.2.1 The n\_TOF facility

The n\_TOF (neutron time of flight) facility is part of the European Organization for Nuclear Research (CERN) and has been operative since 2001 [12]. It is specifically

designed to study neutron-nucleus interactions.

The n\_TOF facility has a pulsed neutron source coupled with a 200 m flight path. Neutrons are produced by spallation of 20 GeV/c protons delivered by the CERN Protosynchrotron, impinging on a massive lead target [13]. Proton pulses have a RMS width of 6 ns. Each proton yields around 300 neutrons, which are slowed down by an initial 1 cm layer of demineralised water, followed by a second layer of 4 cm of borated water ( $\text{H}_2\text{O} + 1.28\% \text{H}_3\text{BO}_3$ , mass fraction). These layers serve as moderators: the initial fast neutron spectrum becomes an isothergic neutron beam (uniform in lethargy units). Along the 185 m path to the experimental area, collimators are used to shape the neutron beam, magnets are employed to remove charged particles from the beam and shields are used to reduce the background from the spallation source. The available energy resolution at  $E \simeq 1 \text{ keV}$  is  $\Delta E/E \simeq 10^{-4}$  (i.e. smaller than the total width of neutron resonances). Thanks to the Protosynchrotron low duty cycle ( $\sim 1 \text{ Hz}$ ), the overlap between the lowest neutrons of a beam and the fastest neutrons of the following beam is avoided.

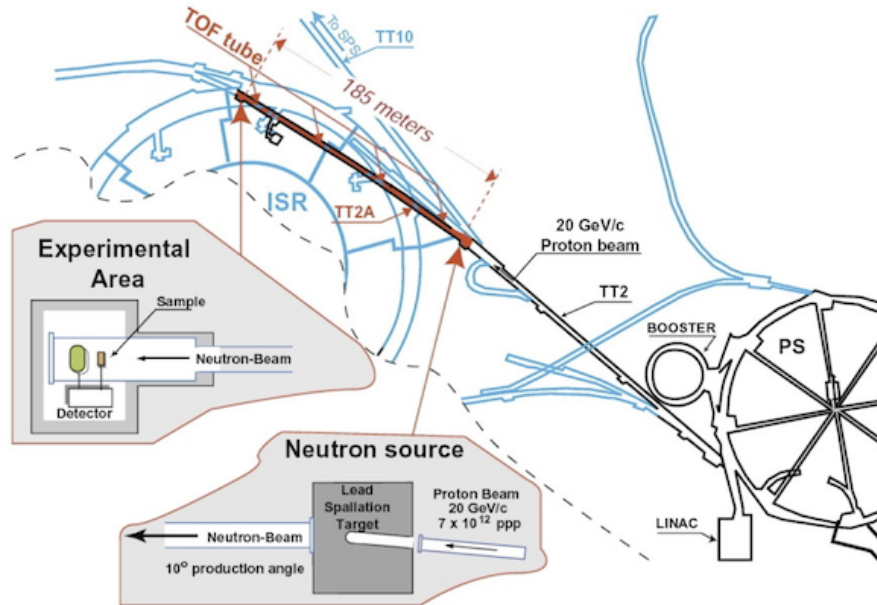


Figure 1.3: n\_TOF facility and Protosynchrotron overview, from CERN [12].

Of the  $2 \cdot 10^{15}$  neutrons/pulse produced at the source,  $1.5 \cdot 10^7$  neutrons/pulse arrive at the sample position and the beam profile is 2 cm in diameter. The experimental area where the samples are positioned is known as EAR1. A schematic view of the facility is represented in Figure 1.3.

## 1.2.2 Experimental setup and Data analysis

For the measurement of  $^{155,157}\text{Gd}(n,\gamma)$  cross-sections at the n\_TOF facility [14], an array of 4 special  $\text{C}_6\text{D}_6$  detectors was used. The deuterated benzene liquid scintillation detectors are particularly suited for  $(n,\gamma)$  measurements and were optimised in order to achieve a low sensitivity to background signal from neutron scatter-

ing. They were put around 10 cm away from the Gd sample, at 90° angles from each other. These organic detectors are very fast and enable measurements on high-energy neutrons. However, they have very low efficiency, and therefore special analysis techniques are required (see Mastromarco et al. [14] and Rocchi and Castelluccio [15]).

The Gd samples were produced by the National Isotope Development Center (NIDC), ORNL, USA, in the form of metallic disks with 1 cm radii. Two thin samples were used to measure  $^{155,157}\text{Gd}$  cross-sections near thermal neutron energy, avoiding saturation of the capture yield due to self-shielding. Thicker samples (10× for  $^{155}\text{Gd}$  and 40× for  $^{157}\text{Gd}$ ) were used for the measurement of cross-sections for neutron energies above 1 eV. A total of 4 high purity (88.32% for  $^{157}\text{Gd}$  and 91.74% for  $^{155}\text{Gd}$ ) samples was used for the campaign.

Without claiming to be exhaustive, an overview of the main features and results of the data analysis performed is presented here. For a neutron absorption experiment, we may define the *capture yield* as the fraction of neutron beam that undergoes capture reactions in the gadolinium sample. In particular, for this experiment, for some energy  $E_n$  we have

$$Y(E_n) = \frac{N}{S_n + E_n \frac{A}{A+1}} \cdot \frac{C_w(E_n) - B_w(E_n)}{\varphi_n(E_n) f_{BIF}(E_n)}. \quad (1.1)$$

The first factor in Eq. 1.1 contains a normalisation factor  $N$ , the neutron separation energy of the compound nucleus  $S_n$  and the mass number of the target nucleus  $A$ . In the second factor, then,  $C_w$  is the weighted  $\text{C}_6\text{D}_6$  counting rate,  $B_w$  is the weighted background count rate,  $\varphi_n$  is the neutron fluence and  $f_{BIF}$  (Beam Interception Factor) is a correction factor taking into account the variation of the neutron-beam profile (and therefore interception with the sample) as a function of the neutron energy.

It is worth mentioning that the total-energy detection principle was applied for the present analysis. Therefore the detection efficiency was “artificially” set proportional to the incoming  $\gamma$ -ray energy through the pulse height weighting technique. For a complete discussion of the n\_TOF Gd campaign, the reader is referred to Mastromarco et al. [14].

From the measured capture yield results, it was possible to calculate a value for  $^{157}\text{Gd}$  at the thermal point of  $239.8 \pm 9.3$  kb (1 standard deviation) [3], reported in Fig. 1.2. This point lies between the Mughabghab [7] evaluation of  $254$  kb  $\pm 0.3\%$  and the Leinweber et al. [5] evaluation of 226 kb. Through the implementation of the resonance parameters calculated with the n\_TOF campaign, ACE format<sup>3</sup> nuclear data files have been produced for isotopes  $^{155,157}\text{Gd}$  and were used for the simulations presented in this work (see Section 3.5).

---

<sup>3</sup>The ACE file format (A Compact ENDF) is a continuous-energy standard format for MCNP simulations.

# Computational Methods

In this chapter, the computational methods employed for the benchmark simulations discussed in Chapter 3 in the context of reactor criticality calculations will be introduced. In the following sections, the mathematical framework of the eigenvalue problem will be introduced and the power iteration solution technique will be discussed. The sensitivity and uncertainty theory will be summarised and, finally, the MCNP code examined and its main features listed, with a focus on its mathematical methods.

## 2.1 The eigenvalue problem

For the assessment of gadolinium poisoning as a reactor safety device, we are interested in the benchmarking of a selected case study (see Chapter 3) in order to quantify the effect of the gadolinium injection into a reactor core. In order to measure the effect of the poison on the behaviour of the reactor, we consider a macroscopic parameter called *effective multiplication factor*,  $k_{eff}$ . Physically, it represents the ratio of neutrons between two consequent “generations”. If  $k_{eff} = 1$ , the reactor core is *critical*, whereas if  $k_{eff} > 1$  or  $k_{eff} < 1$  the reactor core is, respectively, *super-critical* and *subcritical*. In general, we refer to the calculations of  $k_{eff}$  as *criticality calculations*.

Mathematically, the  $k_{eff}$  factor equation arises from a quite complicated derivation, which is omitted here. Rather, the following discussion begins with the special case considered in this work. The benchmark problem analysed in Chapter 3 is in fact the case of a stationary reactor, i.e. a reactor where the neutronics are constant in time. Let us then straight-forwardly introduce the neutron transport equation relative to our case study, namely a time-independent neutron transport equation [16]:

$$\begin{aligned}
 \left[ \vec{\Omega} \cdot \nabla + \Sigma_T(\vec{r}, E) \right] \Psi_k(\vec{r}, E, \vec{\Omega}) &= \\
 &= \iint \Psi_k(\vec{r}, E', \vec{\Omega}') \Sigma_S(\vec{r}, E' \rightarrow E, \vec{\Omega} \cdot \vec{\Omega}') d\vec{\Omega}' dE' \quad (2.1) \\
 &+ \frac{1}{k_{eff}} \cdot \frac{\chi(E)}{4\pi} \iint \nu \Sigma_F(\vec{r}, E') \Psi_k(\vec{r}, E', \vec{\Omega}') d\vec{\Omega}' dE'.
 \end{aligned}$$

Note that the equation above, in fact, contains the  $k_{eff}$  factor on the right-hand-side. Let us first examine the meaning of each term in Equation 2.1:

- $\vec{\Omega}$  is the versor indicating the direction of motion of neutrons;
- $E$  is the energy;
- $\vec{r}$  is the position vector;
- $\Psi_k(\vec{r}, E, \vec{\Omega})$  is the time-independent neutron flux density at position  $\vec{r}$ , for particles with energy  $E$ , moving in direction  $\vec{\Omega}$  (the  $k$  subscript denotes a  $k_{eff}$  eigenvalue calculation);
- $k_{eff}$  is the effective multiplication factor;
- $\chi(E)$  is the energy probability density function for fission neutrons (i.e. the neutron fission spectrum), including both prompt and delayed neutrons;
- $\nu$  is the average number of neutrons per fission event;
- $\Sigma_T(\vec{r}, E)$  is the macroscopic total neutron cross-section at position  $\vec{r}$  and energy  $E$ ;
- $\Sigma_S(\vec{r}, E' \rightarrow E, \vec{\Omega} \cdot \vec{\Omega}')$  is the double differential macroscopic scattering cross-sections for neutrons with energy  $E'$  and direction of motion  $\vec{\Omega}'$  to energy  $E$  and direction  $\vec{\Omega}$ ;
- $\Sigma_F(\vec{r}, E')$  is the macroscopic fission cross-section at position  $\vec{r}$  and energy  $E'$ .

Equation 2.1 expresses a neutron balance, by identifying four terms, each expressing a gain or a loss of neutrons in the point of the phase space. Each of these four terms can be expressed as an operator acting on the vector  $\Psi_K$ : a detailed explanation of the symbols is shown in Table 2.1. This useful notation allows one to rewrite Equation 2.1 as:

$$\left(\hat{L} + \hat{T}\right) \Psi = \hat{S}\Psi + \frac{1}{k_{eff}} \hat{M}\Psi \quad (2.2)$$

where  $\Psi$  summarises  $\Psi_k$  in each point  $(\vec{r}, E, \vec{\Omega})$ . With some more manipulation we have:

$$\Psi = \frac{1}{k_{eff}} \cdot \left(\hat{L} + \hat{T} - \hat{S}\right)^{-1} \hat{M}\Psi \quad (2.3)$$

and, with  $\hat{F} \equiv \left(\hat{L} + \hat{T} - \hat{S}\right)^{-1} \hat{M}$ , we may write:

$$\Psi = \frac{1}{k_{eff}} \cdot \hat{F}\Psi. \quad (2.4)$$

Equation 2.4 is clearly an *eigenvalue equation*, where  $\Psi$  is the eigenvector and  $k_{eff}$  is the eigenvalue.

So far, the problem has been described mathematically. Now it will be possible to find a solution with respect to the parameters  $\Psi$  and  $k_{eff}$ . The technique adopted is the *power iteration method*.

Operator Name	Notation	Equation Term	Description
Leakage Operator	$\hat{L}\Psi_k(\vec{r}, E, \vec{\Omega})$	$\vec{\Omega} \cdot \nabla \Psi_k(\vec{r}, E, \vec{\Omega})$	Number of neutrons that leave from the point in the phase space $(\vec{r}, E, \vec{\Omega})$
Collision Operator	$\hat{T}\Psi_k(\vec{r}, E, \vec{\Omega})$	$\Sigma_T(\vec{r}, E) \Psi_k(\vec{r}, E, \vec{\Omega})$	Number of neutrons colliding at $(\vec{r}, E, \vec{\Omega})$
Scatter-in Operator	$\hat{S}\Psi_k(\vec{r}, E, \vec{\Omega})$	$\iint \Psi_k(\vec{r}, E', \vec{\Omega}') \cdot \Sigma_S(\vec{r}, E' \rightarrow E, \vec{\Omega} \cdot \vec{\Omega}') \cdot d\vec{\Omega}' dE'$	Number of neutrons that scatter scatter to $(\vec{r}, E, \vec{\Omega})$
Multiplication fission Operator	$\hat{M}\Psi_k(\vec{r}, E, \vec{\Omega})$	$\frac{\chi(E)}{4\pi} \iint \nu \Sigma_F(\vec{r}, E') \cdot \Psi_k(\vec{r}, E', \vec{\Omega}') d\vec{\Omega}' dE'$	Number of neutrons produced by fission $\times k_{eff}$ at $(\vec{r}, E, \vec{\Omega})$

Table 2.1: Description of the terms in Eq. 2.1 and associated operator symbols.

### 2.1.1 Power Iteration

The principle behind the power iteration method is to iterate the eigenvalue calculation until stable values are obtained for both  $k_{eff}$  and  $\Psi$ . Let us then introduce the indexed eigenvector  $\Psi^{(n)}$  and the indexed eigenvalue  $k_{eff}^{(n)}$ .

Assuming that  $\Psi$  and  $k_{eff}$  are known for iteration (n), we may make an estimate of  $\Psi^{(n+1)}$  according to:

$$\Psi^{(n+1)} = \frac{1}{k_{eff}^{(n)}} \cdot \hat{F}\Psi^{(n)}. \quad (2.5)$$

From the equation above, we have

$$\left(\hat{L} + \hat{T} - \hat{S}\right) \Psi^{(n+1)} = \frac{1}{k_{eff}^{(n)}} \cdot \hat{M}\Psi^{(n)} \quad (2.6)$$

and, of course, the following also holds:

$$\left(\hat{L} + \hat{T} - \hat{S}\right) \Psi^{(n+1)} = \frac{1}{k_{eff}^{(n+1)}} \cdot \hat{M}\Psi^{(n+1)}. \quad (2.7)$$

Through the right-hand-sides of both equations 2.6 and 2.7, we can estimate  $k_{eff}^{(n+1)}$ :

$$k_{eff}^{(n+1)} = k_{eff}^{(n)} \frac{\int \hat{M}\Psi^{(n+1)} d\vec{r}}{\int \hat{M}\Psi^{(n)} d\vec{r}}. \quad (2.8)$$

The equation above uses the  $\hat{M}$  operator for normalisation purposes. However, the choice of the normalisation operator is arbitrary, and other choices could be made, according to Equation 2.6.

This iterative method only requires an initial estimate of  $\Psi$  and  $k_{eff}$ . The iterations continue until both the eigenvector and eigenvalue have asymptotically converged.

### 2.1.2 Convergence assessment

We are now interested in assessing the behaviour of the source eigenvector  $\Psi$  and eigenvalue  $k_{eff}$ . Let us expand  $\Psi$  in terms of the orthonormal eigenfunctions  $\vec{u}_j$ :

$$\Psi = \sum_{j=0} a_j \vec{u}_j \quad (2.9)$$

with  $\int \vec{u}_j \vec{u}_k dV = \delta_{jk}$  and  $a_j = \int \Psi \cdot \vec{u}_j dV$ . It is known from linear algebra that there exist one dominant eigenvalue  $k_0 \equiv k_{eff}$  such that  $k_0 > k_1 > k_2 > \dots$

Then, rewriting Equation 2.4 in light of the spectral decomposition of Equation 2.9, we have:

$$\vec{u}_j = \frac{1}{k_j} \hat{F} \cdot \vec{u}_j. \quad (2.10)$$

Finally, we can write an expression for  $\Psi^{(n+1)}$  using both the power iteration and the expansion:

$$\Psi^{(n+1)} = \frac{1}{k^{(n)}} \hat{F} \cdot \Psi^{(n)} = \frac{1}{k^{(n)}} \cdot \frac{1}{k^{(n-1)}} \cdot \dots \cdot \frac{1}{k^{(0)}} \cdot \hat{F}^{n+1} \Psi^{(0)} \quad (2.11)$$

and expanding  $\Psi^{(0)}$  in the eigenbasis we have

$$\begin{aligned} \Psi^{(n+1)} &= \prod_{m=0}^n \frac{1}{k^{(m)}} \cdot \hat{F}^{n+1} \cdot \sum_{j=0} a_j^{(0)} \vec{u}_j = \prod_{m=0}^n \frac{1}{k^{(m)}} \cdot \sum_{j=0} a_j^{(0)} \cdot \hat{F}^{n+1} \vec{u}_j = \\ &= \prod_{m=0}^n \frac{1}{k^{(m)}} \sum_{j=0} a_j^{(0)} k_j^{n+1} \vec{u}_j = \prod_{m=0}^n \frac{k_0}{k^{(m)}} \sum_{j=0} a_j^{(0)} \frac{k_j^{n+1}}{k_0^{n+1}} \vec{u}_j = \\ &= \prod_{m=0}^n \left( \frac{k_0}{k^{(m)}} \right) \cdot a_0^{(0)} \left( \vec{u}_0 + \sum_{j=1} \frac{a_j^{(0)}}{a_0^{(0)}} \left( \frac{k_j}{k_0} \right)^{n+1} \vec{u}_j \right) \simeq \\ &\simeq [const.] \left( \vec{u}_0 + \frac{a_1^{(0)}}{a_0^{(0)}} \cdot \left( \frac{k_1}{k_0} \right)^{n+1} \cdot \vec{u}_1 + \frac{a_2^{(0)}}{a_0^{(0)}} \cdot \left( \frac{k_2}{k_0} \right)^{n+1} \cdot \vec{u}_2 + \dots \right). \end{aligned} \quad (2.12)$$

According to Equation 2.8, then, we can calculate  $k^{(n+1)}$ :

$$k^{(n+1)} \simeq k_0 \cdot \frac{\left[ 1 + \left( \frac{a_1^{(0)}}{a_0^{(0)}} \right) \cdot \left( \frac{k_1}{k_0} \right)^{n+1} \cdot G_1 + \left( \frac{a_2^{(0)}}{a_0^{(0)}} \right) \cdot \left( \frac{k_2}{k_0} \right)^{n+1} \cdot G_2 + \dots \right]}{\left[ 1 + \left( \frac{a_1^{(0)}}{a_0^{(0)}} \right) \cdot \left( \frac{k_1}{k_0} \right)^n \cdot G_1 + \left( \frac{a_2^{(0)}}{a_0^{(0)}} \right) \cdot \left( \frac{k_2}{k_0} \right)^n \cdot G_2 + \dots \right]} \quad (2.13)$$

where

$$G_m = \frac{\int \hat{M} \vec{u}_m d\vec{r}}{\int \hat{M} \vec{u}_0 d\vec{r}}. \quad (2.14)$$

Equations 2.12 and 2.13 can provide insights into the evolution of the source  $\Psi$  and eigenvalue  $k_{eff}$  as the iterations proceed. In fact, since we imposed  $k_0 = k_{eff}$  to be the highest of the eigenvalues for the set of possible modes, the factors  $(k_j/k_0)^n$  will all tend to zero, as  $n$  tends to infinity. Therefore, for  $n \rightarrow +\infty$ ,  $\Psi^{(n)} \rightarrow \vec{u}_0$  and  $k^{(n)} \rightarrow k_0$  (the fundamental eigenmode and eigenvalue, respectively).

However,  $\Psi$  and  $k_{eff}$  do not converge with the same pace. Let us define the *dominance ratio* DR as the ratio between the first and the fundamental mode eigenvalues

$$\text{DR} = \frac{k_1}{k_0} \quad (2.15)$$

which, as we just mentioned, is smaller than 1, because  $k_1 < k_0$ . Since the terms due to higher modes die off quickly, the dominance ratio is the main source of error in  $\Psi^{(n)}$ . An additional approximation may be made on  $k^{(n+1)}$ :

$$\begin{aligned} k^{(n+1)} &\simeq k_0 \cdot \frac{\left[ 1 + \left( \frac{a_1^{(0)}}{a_0^{(0)}} \right) \cdot \left( \frac{k_1}{k_0} \right)^{n+1} \cdot G_1 + \left( \frac{a_2^{(0)}}{a_0^{(0)}} \right) \cdot \left( \frac{k_2}{k_0} \right)^{n+1} \cdot G_2 + \dots \right]}{\left[ 1 + \left( \frac{a_1^{(0)}}{a_0^{(0)}} \right) \cdot \left( \frac{k_1}{k_0} \right)^n \cdot G_1 + \left( \frac{a_2^{(0)}}{a_0^{(0)}} \right) \cdot \left( \frac{k_2}{k_0} \right)^n \cdot G_2 + \dots \right]} \simeq \\ &\simeq k_0 \left[ 1 + \left( \frac{a_1^{(0)}}{a_0^{(0)}} \right) \cdot \left( \frac{k_1}{k_0} \right)^{n+1} \cdot G_1 \right] \left[ 1 - \left( \frac{a_1^{(0)}}{a_0^{(0)}} \right) \cdot \left( \frac{k_1}{k_0} \right)^n \cdot G_1 \right] \simeq \\ &\simeq k_0 \left[ 1 + \left( \frac{a_1^{(0)}}{a_0^{(0)}} \right) \cdot \left( \frac{k_1}{k_0} \right)^n \cdot \left( \frac{k_1}{k_0} - 1 \right) \cdot G_1 \right] \end{aligned} \quad (2.16)$$

where we notice that an additional  $(k_1/k_0 - 1)$  multiplies the DR term. For typical light-water reactor systems, the DR is in the range 0.8 – 0.99 [17], so the  $(\text{DR} - 1)$  factor is not small enough to entail immediate convergence of  $k_{eff}$ . For some other critical systems, though, the DR can be very close to one. In such cases, the  $k_{eff}$  multiplication factor converges very rapidly compared to the fission source  $\Psi$  and additional care is needed in assessing convergence [18]. For this reason, we always couple the  $k_{eff}$  calculation to a measure of the source convergence, computing the *Shannon entropy* of the source distribution [18].

A 3D grid is superimposed on the system and a number of boxes is considered, in order to have a minimum amount of entries per box. The Shannon entropy of the discretised source distribution is a sum over all of the  $N$  boxes:

$$H_{SRC} = - \sum_{J=1}^N P_J \cdot \ln_2(P_J), \quad (2.17)$$

where  $P_J$  is the ratio between the number of source sites in the  $J$ -th grid box and the total number of source sites. The two limit cases for  $H_{SRC}$  are a point distribution, where  $H_{SRC} = 0$ , and the uniform distribution, where  $H_{SRC} = \ln_2(P_J)$ .

The concepts illustrated in this section will be examined in the following sections of this chapter in the context of the MCNP code.

## 2.2 Sensitivity and uncertainty analysis

Let us now describe the mathematical framework of the sensitivity and uncertainty theory.  $k_{eff}$  physically represents the ratio between the number of neutrons in the  $i_{th}+1$  generation and those in the  $i_{th}$  generation. Mathematically,  $k_{eff}$  is an integral parameter (see previous section), and is a function of several reactor parameters:

$$k_{eff} = f(x_1, x_2, \dots, x_N) \quad (2.18)$$

For the purpose of this work's simulations, though, the multiplication factor can be considered as a function of the isotopes cross-sections only, as they will be the only parameters being affected during the MCNP code execution (see Section 2.3). In fact, the sensitivity is computed by means of the perturbation theory, perturbing the targeted cross-sections. Overall, for  $n$  isotopes, we have:

$$k_{eff} = f(\sigma_1, \dots, \sigma_n). \quad (2.19)$$

Considering small deviations, it is possible to expand in a Taylor series. Truncating to first order we have

$$k_{eff}(\sigma_1, \dots, \sigma_n) \simeq k_{eff}(\sigma_{i0}, \dots, \sigma_{n0}) + \sum_{i=1}^n \left( \frac{\partial k_{eff}}{\partial \sigma_i} \right)_{\sigma_{i0}} (\sigma_i - \sigma_{i0}) \quad (2.20)$$

so that the differential is

$$dk_{eff} = \sum_{i=1}^n \left( \frac{\partial k_{eff}}{\partial \sigma_i} \right)_{\sigma_{i0}} (\partial \sigma_i). \quad (2.21)$$

Then taking the ratio  $dk_{eff}/k_{eff}$  we may write

$$\frac{dk_{eff}}{k_{eff}} = \sum_{i=1}^n \left( \frac{\partial k_{eff}}{\partial \sigma_i} \right)_{\sigma_{i0}} \frac{\partial \sigma_i}{\sigma_{i0}} \frac{\sigma_{i0}}{k_{eff}} = \sum_{i=1}^n \left( \frac{\partial k_{eff}/k_{eff}}{\partial \sigma_i/\sigma_{i0}} \right) \Big|_{\sigma_{i0}} \frac{\partial \sigma_i}{\sigma_{i0}} \quad (2.22)$$

and we define the **sensitivity coefficients**

$$S_i = \left( \frac{\partial k_{eff}/k_{eff}}{\partial \sigma_i/\sigma_{i0}} \right) \Big|_{\sigma_{i0}} \quad (2.23)$$

which yield

$$\frac{dk_{eff}}{k_{eff}} = \sum_{i=1}^n S_i \Big|_{\sigma_{i0}} \cdot \frac{\partial \sigma_i}{\sigma_{i0}}. \quad (2.24)$$

Equation 2.24 represents the type of calculation carried out in this work with the evaluation of benchmarks for sensitivity analyses. In particular, in our benchmarking problem (discussed in Chapter 3), the  $k_{eff}$  sensitivity is calculated with respect to the isotopes  $^{155}\text{Gd}$  and  $^{157}\text{Gd}$ , one at a time, so that the sum in Eq. 2.24 reduces to one single term. Two types of such calculations are carried out: energy-dependent sensitivity calculations, and integral sensitivity calculations (over the whole energy spectrum), which we expect to be equal. In the next section, the code used for the benchmarking process is examined together with the sensitivity analysis calculational tools. The benchmark calculation setup is then reported in Section 3.2.

## 2.3 MCNP code

The benchmark calculations were carried out with MCNP6.2 code, run on CRESCO systems (part of the ENEA calculational infrastructure).

MCNP (Monte Carlo N-Particle) is a general purpose, continuous energy, generalised geometry, time dependent, Monte Carlo radiation-transport code designed to track many particle types over broad ranges of energies [19]. The Monte Carlo method is a powerful tool to solve complex 3D problems because it is a *statistical* method. It is particularly suited for continuous energy calculations, i.e. the kind performed in this work. It is based on pseudo-random number generation: complex algorithms generate a sequence of numbers, and the difference between sequences is guaranteed by unique *seeds*.

In practice, the code simulates particles in a physical system, and calculates each particle's history throughout each cycle. The code can be operated to transport a wide variety of particles, although for this work it was only requested to transport neutrons (see Section 3.2). For example, a neutron may elastically scatter on a carbon nucleus (n,n) and subsequently fission a  $^{235}\text{U}$  atom (n,f) or undergo radiative capture (n, $\gamma$ ) hitting a poisoning isotope, like gadolinium. A possible path is shown in Fig. 2.1.

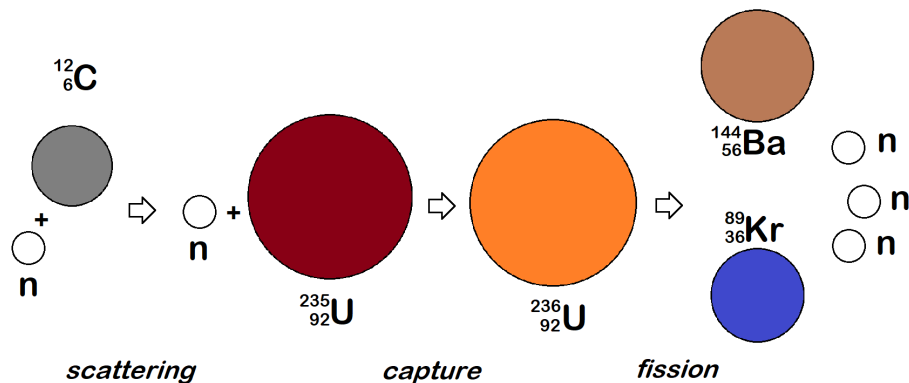


Figure 2.1: Diagram of a neutron elastically scattering on a  $^{12}_6\text{C}$  nucleus, then hitting a  $^{235}_{92}\text{U}$  atom and causing fission. Overall, two more neutrons are released in this process.

For its intrinsically statistical behaviour, the Monte Carlo method is usually the most faithful description of what happens in a real system. On the other hand, though, it takes great computational resources, and only provides the user with the tallies specifically requested (as well as a few default ones).

In comparison, *deterministic* methods, such as the discrete ordinates method, allow one to solve the transport equation for the average particle. A few of these methods (partially deterministic methods) are actually included in the MCNP code, as variance reduction options. However, deterministic methods are not suited for all nuclear reactor systems calculations and, in the case of the benchmarks presented in

this work, Monte Carlo stochastic methods are employed [17]. Let us now describe the types of structures supported by the MCNP code and the elements employed for the criticality calculations of our benchmarking problem.

The MCNP code is based on one input file, containing the details of the problem. The declarations are structured in *cards*, which represent the statements for the MCNP code. The problem is defined according to a fixed-order structure, whose elements are:

- Geometry (surfaces and cells)
- Materials
- Simulation parameters (the type of calculation and the physical parameters)
- Variance reduction parameters

### 2.3.1 Criticality calculations

Two different types of calculations are permitted: defined source calculations and eigenvalue calculations. The former type is used when the source is known and consequently does not change throughout the problem. The latter is used when the particle source is unknown and to be found within the problem execution by solving an eigenvalue problem. This represents the type of calculation performed in this work. Hence, a so-called KCODE source is used. The user can define the number of histories (source particles) per cycle, and the number of cycles to evaluate.

The so-called KSRC card is then required to choose the position of the first generation of neutrons, which have to be in the vicinity of fission sites. The specified  $k_{eff}$  and KSRC are computational representations of the initial estimates for the eigenvalue and eigenvector as part of a power iteration eigenvalue problem (see Section 2.1).

When a job is run, the code initially generates the specified number of histories (according to KSRC) and processes the first cycle. After the first cycle has ended, some neutrons will have disappeared (for example, due to neutron absorption), and some new ones will have been created. Then, in order to keep the reactor critical, the code generates just *as many neutrons as initially requested*, from the spatial points where the previous neutrons have been terminated, typically “adding” some new ones.  $k_{eff}$  is calculated for each iteration, and at the end of the simulation, the *average  $k_{eff}$*  is given with its associated uncertainty.

Three types of estimators are used for the calculation of  $k_{eff}$ : collision, absorption and track-length estimators. They represent different ways of calculating the effective multiplication factor, and the average of the three (each averaged over the number of executed cycles) is taken as the “result” at the end of a criticality calculation. The results of the KCODE calculations performed for the selected benchmark are examined in the following chapter.

### 2.3.2 Tallies

Other physical quantities (*tallies*) are also calculated averaging over all of the cycles and, again, what happens to each particle is due to the probability of each possible outcome in the simulated random walk. Tallies are simply calculated by counting the number of particles that behave in some specific way. Qualitatively, one might make an estimate of the particle flux in a point of the system geometry by counting how many particles collide in a nearby cell.

Flux is taken as the neutron spectrum in the moderator, averaged over all the considered *cells*, hence taking a spatial average, using the F4 *tally flux* card. The E *tally energy* card is used to specify 237 *energy bins*, ranging from  $10^{-5}$  eV to 20 MeV (usually taken as the high end of a reactor's neutron spectrum). Complementary tally cards are also used to perform the flux calculation.

$k_{eff}$  sensitivity to isotopic cross-section variations is calculated through the so-called KSEN card. The isotope and the data library are specified together with the reaction number. The card can only be used in KCODE calculations and is recommended for code validation and uncertainty qualification [19]. The KSEN card is based on linear perturbation theory. It is specifically designed for *continuous energy* calculations (the kind performed in this work) and could in principle also be used for *multigroup* calculations, although neglecting the effect of cross-section self-shielding.

# ZED-2 Reactor Benchmarks

In this chapter we examine the ZED-2 reactor benchmark calculations with data from the ENDF/B-VII.1 library. Problem setup and calculation details are presented and the results of the simulations are provided. The focus is mainly on reactor sensitivity to Gd odd isotopes' cross-sections. At the end of the chapter, two different data sets are compared, namely data from the ENDF/B-VII.1 library and recently measured n\_TOF (CERN) data. Throughout the chapter, input validation procedures are also discussed.

## 3.1 The ZED-2 reactor

To perform simulations and make predictions on Gd cross-sections data, the ZED-2 reactor was chosen as a case study. It is a thermal neutron spectrum reactor, and experiments were conducted with gadolinium in the reactor core [20], with the results being submitted to the IRPhEP Handbook (International Handbook of Evaluated Reactor Physics Benchmark Experiments), OECD-NEA. Furthermore, a validated ZED-2 reactor core MCNP model was available [21], with simulated  $k_{eff}$  from Chow et al. [21] consistent with experimental  $k_{eff}$  from Atfield [20].

The ZED-2 (Zero Energy Deuterium) reactor (Fig. 3.1) is a heavy water moderated research reactor, operating at the Chalk River Laboratories, AECL, Canada. The ZED-2 reactor is a tank type research reactor, with fuel rods inserted in a cylindrical aluminium tank (calandria), spanning  $\sim 3.4$  m both in height and diameter.

Research reactors differ significantly from commercial power reactors<sup>1</sup>. For instance, the ZED-2 reactor is not connected to turbines or any additional apparatus. It does not need cooling and is usually operated at an indicated power ranging between 5 to 120 watts [22]. Since the reactor produces very little power, the chain reaction is not accountable for a rise in temperature, so the treatment of the reactor kinetics is referred to as *zero-power kinetics*, with a negligible thermal feedback.

Criticality is achieved by varying the heavy water moderator level. As shown in Fig. 3.1 this operation occurs through a system of pumps and valves located below the reactor. The ZED-2 reactor is also equipped with a graphite reflector surrounding the calandria and with a shielding layer all around the core.

---

<sup>1</sup>In general, a power reactor and a research reactor are built for very different purposes: the former needs to guarantee a constant, efficient, reliable heat source, while the latter needs to provide the experimenter with a requested neutron flux.

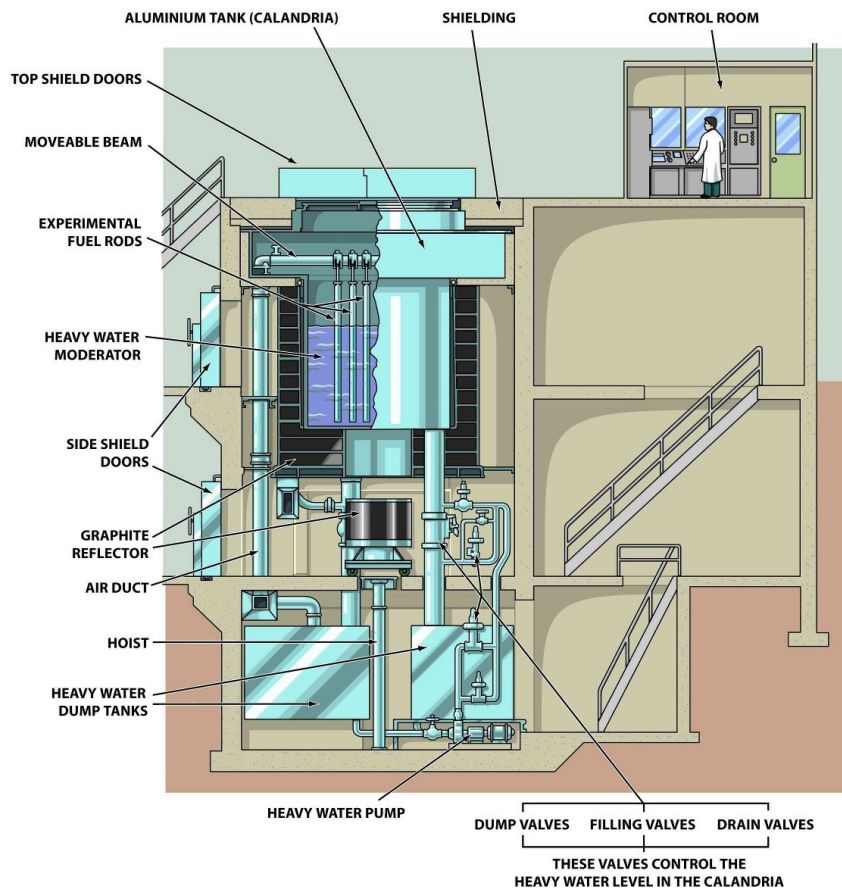


Figure 3.1: Illustration of the ZED-2 Facility in Atfield [20].

The calculations performed for this work involved four different experimental set-ups, each with a different gadolinium concentration. Each set-up is characterised by different parameters, like critical height of moderator, moderator and fuel temperature and moderator purity. These parameters were reported by Chow et al. [21] and will be examined in Section 3.3.

A graphical representation of the ZED-2 core model (from Chow et al. [21]) is shown in Fig. 3.2 via the Visual Editor MCNP code<sup>2</sup>, whereas Table 3.1 presents an overview of the reactor features.

## 3.2 Benchmark calculations

The code input used for the simulations was developed by Chow et al. [21] in the context of ZED-2 reactor benchmarking, following experiments at the ZED-2 facility, Chalk River Laboratories, AECL [20].

The purpose of this section is to examine in detail which settings were chosen for each of the cards introduced in Section 2.3 for the ZED-2 reactor benchmark

<sup>2</sup>The Visual Editor package allows to plot a geometry directly from the MCNP input file (the plot is produced by flooding the geometry with histories).

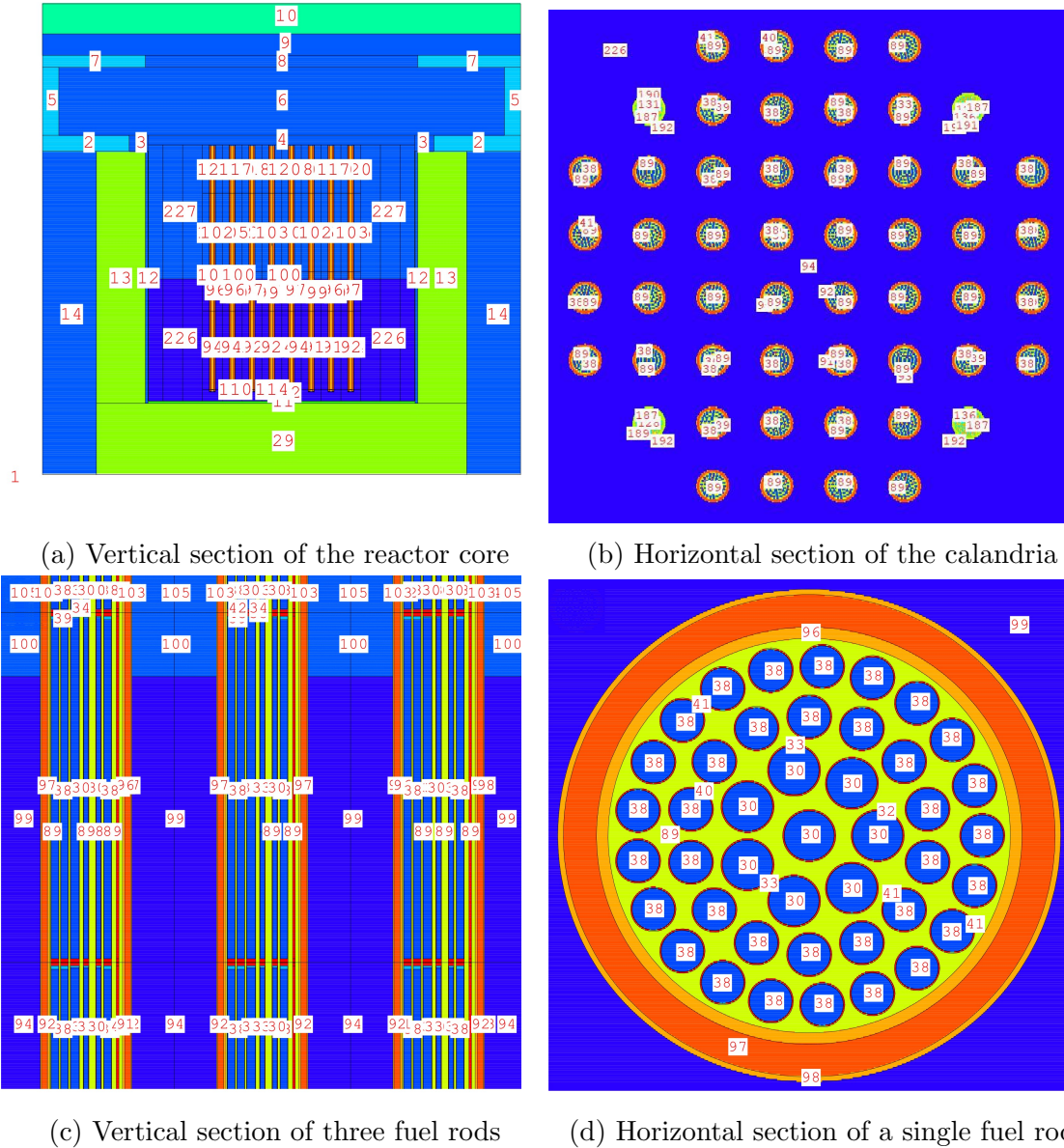


Figure 3.2: ZED-2 reactor core model by J. C. Chow et al., 1.5ppm Gd in the moderator, visualised via the MCNPX Visual Editor, Version X\_24E. Different materials are shown in different colours (for instance the heavy water moderator is shown in dark blue, while air is shown in light blue). The numbers indicate the cells of the system.

problems. Note how we consider the problem of a stationary reactor, with no burn-up, therefore, no change in the isotopic composition is present.

### KCODE criticality calculation card

The KCODE card was used to perform the criticality calculations, simulating 500,000 histories per cycle and 5,000 cycles for each benchmark.

The first calculation performed for this work was the *convergence* check. In

Fuel type	Bundle height	Pitch	Coolant	Moderating system
LEU (Low enriched uranium) / RU (Recovered Uranium)	49.67 cm	24.5 cm pitch square lattice	Stagnant - air cooling	Heavy water moderator

Table 3.1: Overview of the main ZED-2 reactor setup parameters.

order to obtain a reliable calculation it is initially necessary that the effective multiplication factor has converged. Furthermore, the source shape distribution must have also converged to its fundamental mode. In fact, if each cycle began with a significantly different source shape, the tallies calculated during the problem would show great variances and should not be considered safe estimates of the real physical quantities [16].

The standard reference parameter for source distribution convergence in MCNP is the *Shannon entropy* (for a more detailed discussion of the computational tools employed, see Chapter 2). The preliminary checks allowed us to make an estimate of the number of cycles required to achieve  $k_{eff}$  and  $H_{SRC}$  convergence. Hence we set the number of inactive cycles (a KCODE card parameter) to 50 for every subsequent simulation.

Immediately after the KCODE card, the KSRC card also needs be specified, providing an approximated initial source distribution. Below is a summary of the input parameters related to the KCODE card (where, for simplicity, only two rows are shown for the KSRC card).

```

C KCODE NSRCK RKK IKZ KCT
C NSRCK [500,000: number of source histories per cycle]
C RKK   [1: initial guess for keff]
C IKZ = [50: number of cycles to skip before tallying starts]
C KCT = [250: number of cycles to run]
KCODE 500000 1 50 5000
C Initial point sources : one per center of 1st pin in each bundle
C
KSRC   -36.7500  -85.7500   39.2250 $ (0, -3), 1
       -36.7500  -85.7500   88.7350 $ (0, -3), 2
       [...]

```

## HSRC Shannon Entropy card

The KCODE card automatically provides a source entropy calculation together with the estimated  $k_{eff}$  value for each cycle. It does so by automatically superimposing a mesh to the system geometry and estimating the Shannon entropy value for each resulting box.

However, during the code execution, the default mesh is expanded according to the change in the source distribution. Then, in order to gain a better insight into the behaviour of the Shannon entropy for the initial cycles, it is necessary to choose a custom, *fixed* mesh. For this purpose, the HSRC card may be used. The input parameters are the x, y, z ranges for the mesh and the number of cells for each direction. The MCNP6.2 manual recommends the choice of a number of cells equal to the number of histories divided by 20, although not less than  $4 \times 4 \times 4$  should be chosen. For example, with 500,000 histories, a total of  $(30 \times 30 \times 30) \simeq 500,000/20$  cells are chosen. This card was used in particular for the preliminary convergence calculations (see Paragraph 3.4.1). Below is an example of the card in the case of a simulation with 20,000 histories per cycle.

```
HSRC 7 -2.8E+02 2.8E+02 7 -2.8E+02 2.8E+02 7 -1.3E+02 3.2E+02
```

### Physics parameters

The problem was set as a MODE N problem (only neutrons are transported by the code). The PHYS:N card was used to specify neutrons with energies in the range 0 – 20 MeV, and the CUT:N card was used to cutoff neutrons with energies lower than  $10^{-11}$  MeV.

Since in this problem the interest is for a static reactor, no distinction is made between prompt and delayed neutrons. Hence, total  $\bar{\nu}$  factor was used, in order to include both prompt and delayed fission neutrons in the calculation (which is the default choice in the case of KCODE calculations). The TOTNU card is then specified in the code. There are other Physics cards and options which were not specified in the input, therefore the default values were assumed by the code. A summary of the input Physics follows.

```
MODE N
TOTNU
PHYS:N 20 0 0
CUT:N j 1e-11
```

### F4 Flux card

For each simulation, flux tallies are requested. Neutron flux is requested over a broad lattice of moderator cells. In such a way, the whole tank is sampled and a reliable spatially averaged flux can be calculated. In each cell, the flux is binned in 237 energy bins via the E energy card, covering the whole specified neutron spectrum ( $10^{-11}$  MeV – 20 MeV). While flux is calculated over a great number of cells, the total is the quantity of greatest interest, as it is taken as the neutron spectrum in the reactor core. Below, the F4 card is shown as featured in the input, with the brackets used as nested geometry notation and the T indicating the total average.

```
C TALLY FLUX
f14:n (226 < 228[-8:7 -8:7 0] < 229) $ moderator in FA u=19
```

```

(112 < 121 < 228[-8:7 -8:7 0] < 229) $ moderator in FA u= 9
( 94 < 122 < 228[-8:7 -8:7 0] < 229) $ moderator in FA u= 9
( 94 < 123 < 228[-8:7 -8:7 0] < 229) $ moderator in FA u= 9
( 99 < 124 < 228[-8:7 -8:7 0] < 229) $ moderator in FA u= 9
(210 < 219 < 228[-8:7 -8:7 0] < 229) $ moderator in FA u=18
(192 < 220 < 228[-8:7 -8:7 0] < 229) $ moderator in FA u=18
(192 < 221 < 228[-8:7 -8:7 0] < 229) $ moderator in FA u=18
(197 < 222 < 228[-8:7 -8:7 0] < 229) $ moderator in FA u=18
T

```

## KSEN sensitivity calculation card

Finally, the Gd absorption cross-sections sensitivity is calculated for the two Gd odd isotopes ( $^{155,157}\text{Gd}(n,\gamma)$ ) in a number of ways. In particular, for each of the two isotopes, we request both energy binned and integral KSEN calculations. For both of these, we request two different reaction numbers, 102 and special reaction number -2 (radiative neutron absorption and neutron capture, respectively). In the case of gadolinium, these reactions are equivalent, and we expect the two results to be the same. For both of these reactions, we then request both CONSTRAIN=YES and CONSTRAIN=NO calculations. The constrain option is an energy normalisation option only used in fission-chi or scattering law sensitivities and therefore does not affect the calculations considered in our problem.

For each simulation, then, a total of 16 different sensitivity calculations is performed. A summary is represented in Tab. 3.2. The two different reaction numbers and the constrain option are only considered in our problem for consistency check purposes. In other words, as users, it is desirable to verify that these different calculations output the same results. Below is an example of the card, as it was used in the input file (with ksen01 being an integral calculation and ksen05 an energy-dependent calculation).

```

C Integral KSEN
ksen01 xs iso=64157.80c mt=102 -2 constrain=yes
[...]
C Energy dependent KSEN
ksen05 xs iso=6157.80c mt=102 -2 constrain=yes
erg=[...]

```

The simulations were run on the CRESCO6 server (ENEA), where the MCNP6.2 version of the code is installed. For each simulation, 3 cluster nodes were employed, for a total of 144 working CPUs (each node is equipped with 48 Intel(R) Xeon(R) Platinum 8160 CPUs) [23]. In other words, each simulation involved great computational power, and lasted approximately 40 hours. Although the MCNP code offers a great variety of variance reduction techniques, none were used for our problem, thanks to the great computational power offered by the CRESCO server.

Isotope	Binning	Reaction number	Constrain
<sup>157</sup> Gd	No	102	Yes
<sup>157</sup> Gd	No	102	No
<sup>157</sup> Gd	No	-2	Yes
<sup>157</sup> Gd	No	-2	No
<sup>155</sup> Gd	No	102	Yes
<sup>155</sup> Gd	No	102	No
<sup>155</sup> Gd	No	-2	Yes
<sup>155</sup> Gd	No	-2	No
<sup>157</sup> Gd	Yes	102	Yes
<sup>157</sup> Gd	Yes	102	No
<sup>157</sup> Gd	Yes	-2	Yes
<sup>157</sup> Gd	Yes	-2	No
<sup>155</sup> Gd	Yes	102	Yes
<sup>155</sup> Gd	Yes	102	No
<sup>155</sup> Gd	Yes	-2	Yes
<sup>155</sup> Gd	Yes	-2	No

Table 3.2: Summary of the 16 KSEN sensitivity calculations performed for each of the 4 ZED-2 MCNP models. The isotope column indicates the isotope ( $n, \gamma$ ) cross-section which the sensitivity calculation is perturbing. The binning column indicates whether the calculation is energy-dependent (Yes) or integral (No). The constrain column indicates whether the constrain normalisation option is specified. The four blocks separated by horizontal lines are expected to give the same results.

### 3.3 Reactor configurations

In 2006, a team led by Dr. J.E. Atfield carried out experiments at the ZED-2 facility [20]. Following these evaluations, it was possible to develop and calibrate the computational MCNP input models used in this work [21]. For the analyses discussed in the following paragraphs, four different ZED-2 models were evaluated, each with a different gadolinium concentration and different criticality parameters (mainly the heavy water moderator level).

In the first case there is no gadolinium dissolved in the moderator, although small amounts can still be found in the graphite reflector. The second, third and fourth case each come with increasing amounts of dissolved gadolinium. Nominally, the second, third and fourth case have nominal gadolinium concentrations of 0.5 ppm, 1.0 ppm, 1.5 ppm respectively (i.e.  $\mu\text{g}$  of Gd per g of fuel). The details of each experimental reactor configuration examined by Atfield [20] have been summarised by Chow et al. [21]. They are reported in Tab. 3.3

Case	ppm Gd	Moderator Purity [wt%D <sub>2</sub> O]	Channel Temperature [°C]	Moderator Temperature [°C]	Critical Height [cm]
G1	0.0	98.748	21.80	21.70	131.585
G2	0.5	98.748	21.75	21.79	138.248
G3	1.0	98.744	21.65	21.89	145.632
G4	1.5	98.739	21.45	22.51	153.926

Table 3.3: Reactor core parameters for the four MCNP Gd cases, from Chow et al. [21].

### 3.3.1 Model calibration

The nominal gadolinium concentration might differ significantly from the real concentration. In fact, as it happens, the portion of “effective” poison in the reactor tank is always to an extent less than the dissolved amount: small amounts can leave the “active” part of the core and be transported into the pipes connected to the tank, where the neutron flux becomes small. Therefore, a *calibration factor* is introduced to obtain more accurate evaluations of the amount of poison in the moderator. To calibrate the Gd concentration for each case, it is convenient to initially calibrate the concentration of a different element (boron) with reference isotopic cross-sections (i.e. negligible associated error). For each case, criticality is set as a requirement in this approach (since it was initially obtained experimentally) and poison concentrations are corrected consequently. In fact, while the error on boron cross-sections can be considered negligible with respect to the  $k_{eff}$  calculation, there can be a significant bias in the poison concentration, which is hence accountable for deviations from criticality. Once the calibration factor is calculated for a reference element (boron), that same factor can be applied for the element of interest (gadolinium), assuming the same systematic error affects the two concentrations (i.e., that the boron and gadolinium compounds have the same solubility in the heavy water moderator). This whole procedure, referred to as *calibration*, is only sensible under the assumption of  $k_{eff}$  depending linearly from the poison concentration. The

Boron-Calibrated Gd Conc. [ppm]	$k_{eff}$
0.000	0.99788
0.494	0.99766
0.988	0.99759
1.482	0.99713

Table 3.4: Calibrated Gd concentrations, with the calibration factor calculated by the CRL team [21].

work from J.C. Chow et al. [21] provides 4 different cases for calibration, where the experimental setup is mainly left unaltered. Only the reactor parameters listed in Tab. 3.3 and the boron concentration vary from case to case. The work from

Chow used the E70CRL in-house nuclear data library, based on the ENDF/B-VII.0 library. The linearity hypothesis is verified and the resulting calibration factor is  $-1.2\%$ , which is the factor that is also applied to the Gd concentrations and was implemented in our core models. In other words, the  $-1.2\%$  calibration factor was considered for all of the simulations presented in this work, where the target library is the ENDF/B-VII.1 data set. The corrected Gd concentrations can be found in Tab. 3.4 together with the yielded effective multiplication factors.

A more accurate analysis of this problem that takes into account the ENDF/B-VII.1 data set from the beginning of the calibration procedure can be found in Console Camprini et al. [24].

## 3.4 ENDF/B-VII.1 results and data analysis

In this section, the preliminary calculations are examined in the context of convergence assessment. The main results of the complete simulations are then discussed: the reactor core spectrum and the reactor core sensitivity to cross-sections variations, in the case of ENDF/B-VII.1 gadolinium cross-sections data.

### 3.4.1 Convergence

In order to assess the correct convergence of the effective multiplication factor for our reactor core models, convergence<sup>3</sup> calculations were initially carried out. As described in Section 3.2, the HSRC card is added to the input in order to choose a fixed mesh, sampling the source entropy in every region of the reactor core. In particular, we examined the case with the highest dissolved gadolinium concentration (1.5 ppm). The reference nuclear data library considered here is the ENDF/B-VII.1 nuclear data file.

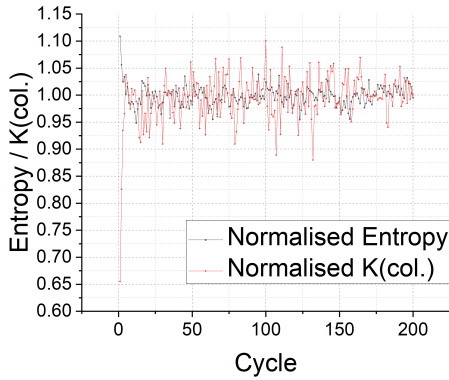
We initially examined a few cases with small numbers of particles. For each case we adjusted the mesh according to the suggested criteria (see Section 3.2). The provided  $k_{eff}$  is calculated solely via the collision estimator. The results of these simulations are plotted in Fig. 3.3. None of these 4 cases actually converge (according to the definition given in footnote 3) because of the relatively small number of particles per cycle and the small number of total cycles. Nevertheless, they intuitively represent the dependence of  $k_{eff}$  and  $H_{SRC}$  fluctuations from the number of particles transported in each cycle.

For the actual simulations that follow, we performed KCODE calculations with 500,000 neutrons per cycle, which yield an almost immediate convergence of both the  $k_{eff}$  factor and the  $H_{SRC}$  entropy, in the first  $\sim 10$  cycles.

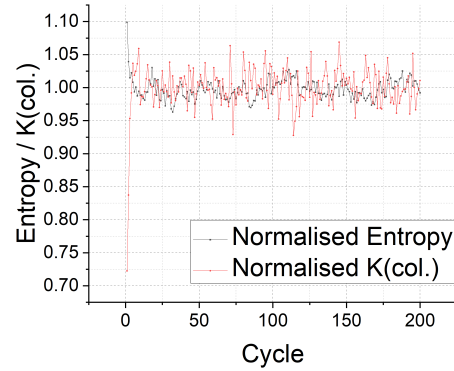
Therefore, making a reasonable safe estimate of the proper number of required inactive cycles, the number was set to 50 for every following simulation.

---

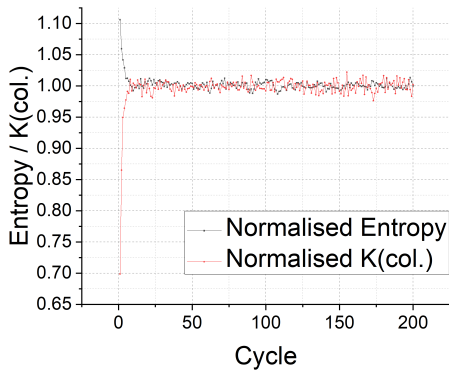
<sup>3</sup> We may talk about convergence with the following convention:  $k_{eff}$  convergence is achieved at some cycle  $n$  if from every following cycle until the last cycle,  $k_{eff}$  is within one standard deviation from the mean of the second half of the  $k_{eff}$  values.



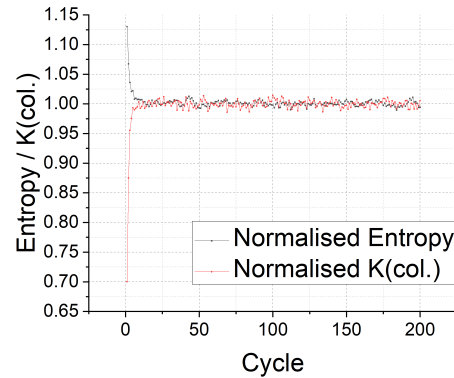
(a) KCODE calculation with 500 particles per cycle. The adopted mesh is the recommended minimum of  $4 \times 4 \times 4$ .



(b) KCODE calculation with 1,000 particles per cycle. The adopted mesh is the recommended minimum of  $4 \times 4 \times 4$ .



(c) KCODE calculation with 10,000 particles per cycle. The adopted mesh is a  $8 \times 8 \times 8$  grid.



(d) KCODE calculation with 20,000 particles per cycle. The adopted mesh is a  $10 \times 10 \times 10$  grid.

Figure 3.3: Results of KCODE calculations in the case with the most dissolved gadolinium, with 500, 1,000, 10,000 and 20,000 particles per cycle respectively. Both  $H_{SRC}$  and  $k_{eff}$  were normalised, so they are comparable in each graph. Each simulation was run for a total of 200 cycles.

### 3.4.2 Neutron Spectra

The four reactor core models introduced in Section 3.3 (summarised in Tab. 3.3) have been benchmarked with complete simulations, with all of the previously introduced features (KCODE, KSEN and tallies) executed at once. The nuclear data library used is again the ENDF/B-VII.1 file. Let us first examine the results of the flux calculations requested via the F4 cards, which are plotted in Figures 3.4 and 3.5.

We may note that the models employed in the calculations really simulate a thermal neutron spectrum, with most neutrons concentrated in the range  $10^{-3}$  eV– $10^{-1}$  eV (which, in fact, is the region with the highest cross-section sensitivities). In addi-

tion, it is shown how increasing amounts of dissolved gadolinium affect the neutron spectrum (Figs. 3.4, 3.5): the peaks around thermal energy are lower for the core models with higher gadolinium concentration. Due to the resolution of the plotted graphs, it is not possible to see the higher fluxes at the right end (high energies) of Figures 3.4 and 3.5. However, the calculated spectra have been correctly normalised<sup>4</sup> according to the calculated integral fluxes and a higher Gd concentration does determine a harder neutron spectrum. This is in accordance with what we would expect, since poisons conceptually “remove” slower neutrons from the reactor core.

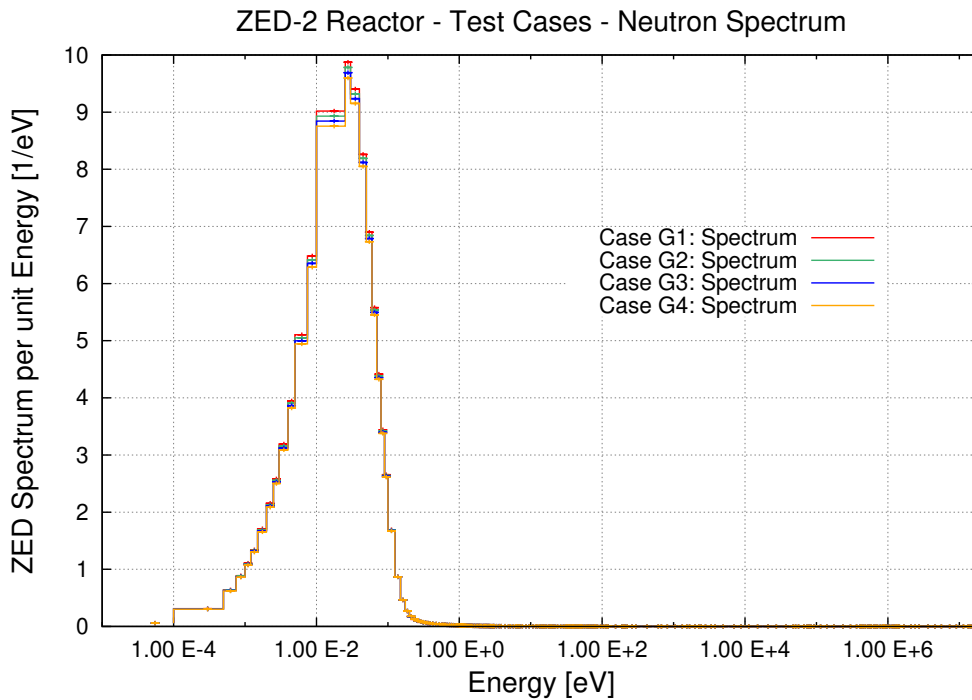


Figure 3.4: Neutron spectrum in the four Gd cases (G1, G2, G3, G4) per unit energy in the ZED-2 reactor core.

### 3.4.3 Sensitivity analysis

From both Figures 3.6 and 3.7 we can see that the reactor is sensitive to Gd cross-section variations, in particular in cases G2, G3 and G4 where the Gd concentration is relevant (note the change of scale from one graph to the other). The sensitivity peak, close to the thermal point, is approximately proportional to the Gd concentration (Fig. 3.7). The sensitivity is generally highest in the near-thermal energy range, particularly from  $10^{-3}$  eV to  $10^{-1}$  eV. The calculations also show that over

<sup>4</sup> Note how here the normalisation procedure is intended solely as a numerical artifact, in order to be able to compare the four examined cases. For the calculation of the simulated core fluxes, one should take into account an additional normalisation factor due to some arbitrary reaction rate. For instance, in KCODE calculations, tallies are normalised to be per fission neutron generation [17].

the whole neutron energy range, the reactor sensitivity to Gd is *negative*: since absorption cross-sections are being considered, a positive cross-section increment yields a negative reactivity worth, i.e. a decrease in the multiplication factor. This behaviour is the standard for poisoning isotopes cross-sections.

The  $^{157}\text{Gd}$  isotope has a greater absorption cross-section than the  $^{155}\text{Gd}$  isotope. This means that the multiplication factor is more sensitive to  $^{157}\text{Gd}(n,\gamma)$  variations than it is to  $^{155}\text{Gd}(n,\gamma)$  variations, as can be seen from Figures 3.6 and 3.7.

The most relevant results from the cases G1, G2, G3, G4 have been listed in Table 3.5.

Case	$k_{eff}$	Integral $^{157}\text{Gd}$ KSEN [dk/d $\sigma$ ]	Integral $^{155}\text{Gd}$ KSEN [dk/d $\sigma$ ]
G1	$0.99557 \pm 0.00001$	$(-2.290 \pm 0.008) \cdot 10^{-5}$	$(-0.533 \pm 0.002) \cdot 10^{-5}$
G2	$0.99542 \pm 0.00001$	$(-0.8352 \pm 0.0003) \cdot 10^{-2}$	$(-1.8744 \pm 0.0007) \cdot 10^{-3}$
G3	$0.99510 \pm 0.00001$	$(-1.6261 \pm 0.0007) \cdot 10^{-2}$	$(-3.6488 \pm 0.0015) \cdot 10^{-3}$
G4	$0.99476 \pm 0.00001$	$(-2.3794 \pm 0.001) \cdot 10^{-2}$	$(-5.339 \pm 0.002) \cdot 10^{-3}$

Table 3.5: Summary of the main calculated parameters for the ZED-2 reactor core MCNP model. The  $k_{eff}$  results are expressed with statistical uncertainty of one standard deviation. The relative uncertainties on KSEN are all around 40 pcm.

While the multiplication factors reported in Table 3.5 indicate that for all four models the reactor core is slightly subcritical as requested, a bias is introduced. In other words, there seems to be an underestimation on the Gd cross-sections, such

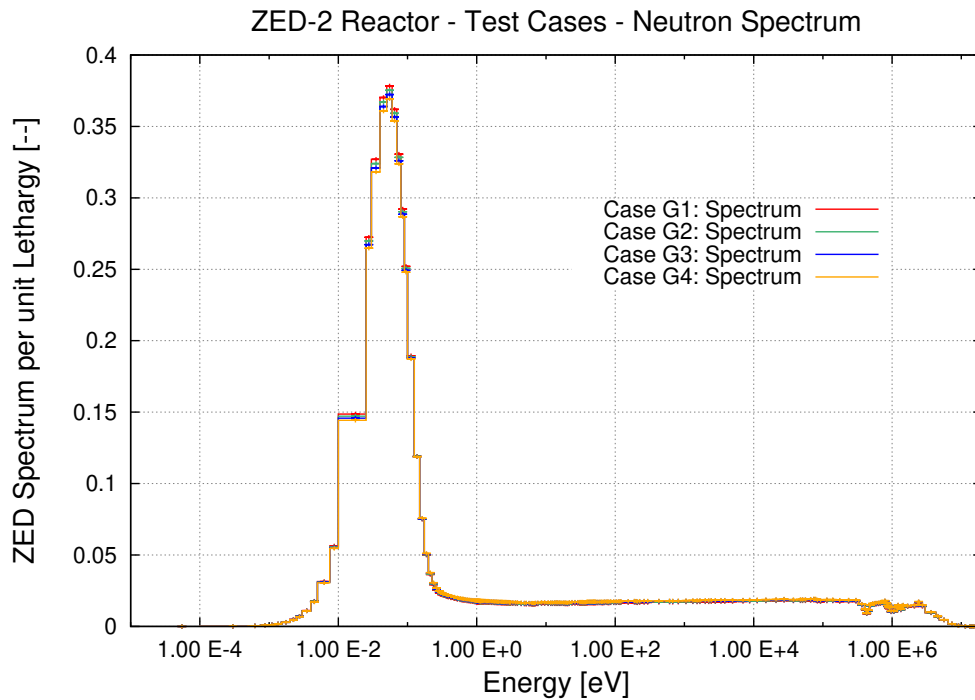


Figure 3.5: Neutron spectrum in the four Gd cases (G1, G2, G3, G4) per unit lethargy in the ZED-2 reactor core.

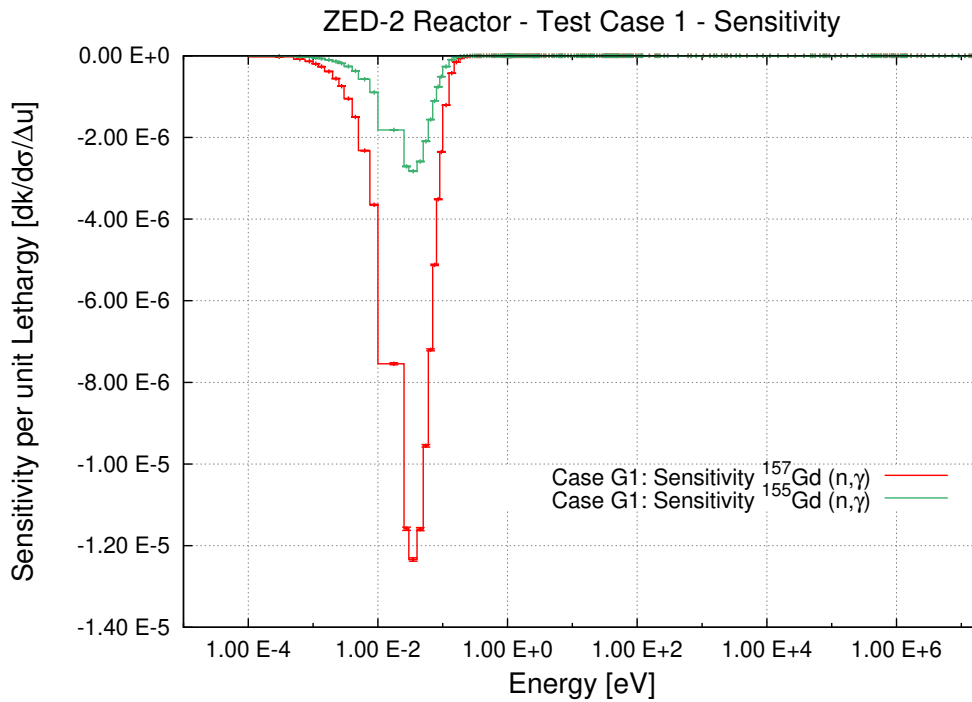


Figure 3.6:  $k_{eff}$  sensitivity to  $^{155,157}\text{Gd}(n,\gamma)$  cross-sections per unit lethargy in case G1 in the ZED-2 reactor core.

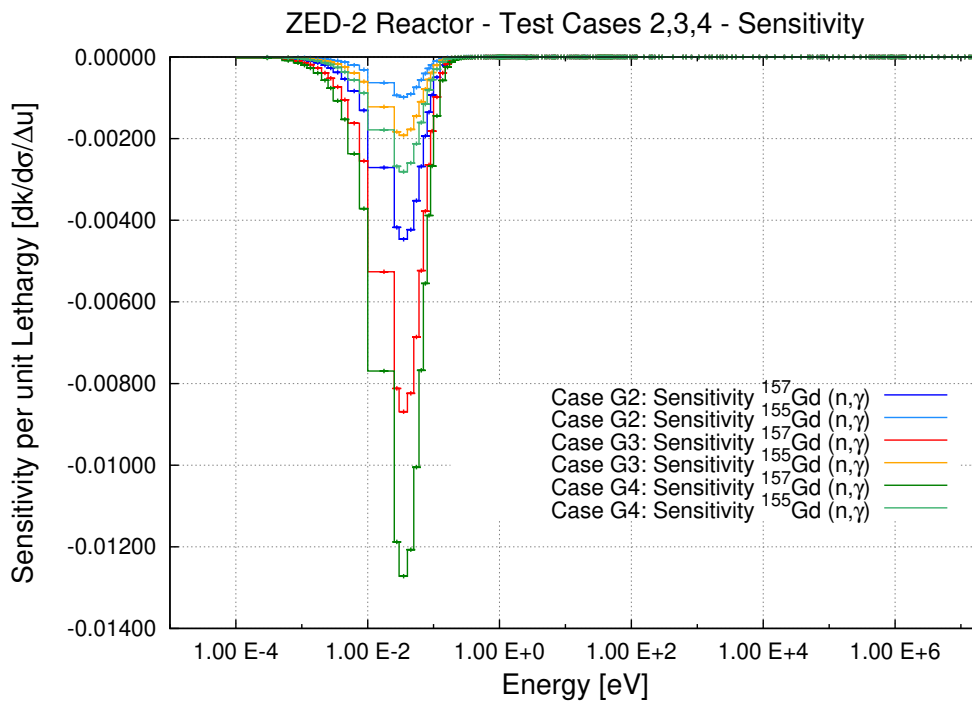


Figure 3.7:  $k_{eff}$  sensitivity to  $^{155,157}\text{Gd}(n,\gamma)$  cross-sections per unit lethargy in cases G2, G3, G4 in the ZED-2 reactor core.

that higher Gd concentrations yield multiplication factors lower than expected. A comparison between the ENDF/B-VII.1 and one of its beta versions (which includes the 2006 Leinweber Gd cross-sections data) can be found in Chow et al. [21]. This matter will also be addressed in Section 3.5, considering the latest available Gd cross-sections data.

Finally, let us examine the code checks introduced in Section 3.2, with reference to Table 3.2, in the context of the KSEN sensitivity calculations. The constrain option showed no effect on the obtained results, with integral and energy-dependent sensitivities being exactly equal in all cases. Similarly, both reaction numbers gave the same results in each of the cases examined, as the Nuclear Physics would suggest.

It is also worth recalling that both the energy-dependent fluxes and the energy-dependent sensitivities can be integrated over the energy range to correctly obtain the MCNP estimate of the integral fluxes and sensitivities, respectively. In fact, the sums of the MCNP energy-binned quantities are in good accordance with the MCNP integral quantities, taken with uncertainty of one standard deviation.

## 3.5 ENDF/B-VII.1 and n\_TOF data comparison

In this last section, the two different Gd data sets (from the ENDF/B-VII.1 library and from the n\_TOF campaign) are compared, in the context of the same KCODE simulations explored in Section 3.4. The aim of this section is to verify whether a bias is introduced in the criticality of the ZED-2 reactor core as more Gd is dissolved in the moderator. The same four cases G1, G2, G3, G4 were run, but the input was modified in order to specify Gd cross-section data reported by Mastromarco et al. [14] (while the rest of the problem still referenced the ENDF/B-VII.1 library). Also, the focus here is only on the criticality of the system, so all of the remaining tallies were excluded, and the adopted input file ended with the KCODE calculation request. The results of these additional calculations are reported in Figure 3.8.

From Figure 3.8 it is immediately understood that there exists a significant bias in the  $k_{eff}$  multiplication factor in the case of ENDF/B-VII.1 Gd cross-sections data, particularly due to  $^{157}\text{Gd}$  cross-section. The bias, given by the slope of the linear fit, is  $-0.45 \pm 0.07$  mk/ppm Gd. Although a smaller bias can still be found in the case of n\_TOF Gd cross-sections data, there is a noticeable improvement. The bias in the n\_TOF data case, opposite in sign, is  $0.19 \pm 0.06$  mk/ppm Gd.

The examined ZED-2 reactor benchmarks suggest that the recently measured  $^{155,157}\text{Gd}(n,\gamma)$  cross-sections represent an improvement, if compared to the ENDF/B-VII.1  $^{155,157}\text{Gd}(n,\gamma)$  cross-sections.

### 3.5.1 $k_{eff}$ Uncertainties

In this paragraph, a method to estimate the uncertainties associated to the final values of the effective multiplication factor is examined. According to Chow et al. [21], we may assess the uncertainty on  $k_{eff}$  as

$$\sigma_{k_{eff}} = \sqrt{\sigma_{stat}^2 + \sigma_{exp}^2 + \sigma_{cal}^2 + \sigma_{Gd}^2} \quad (3.1)$$

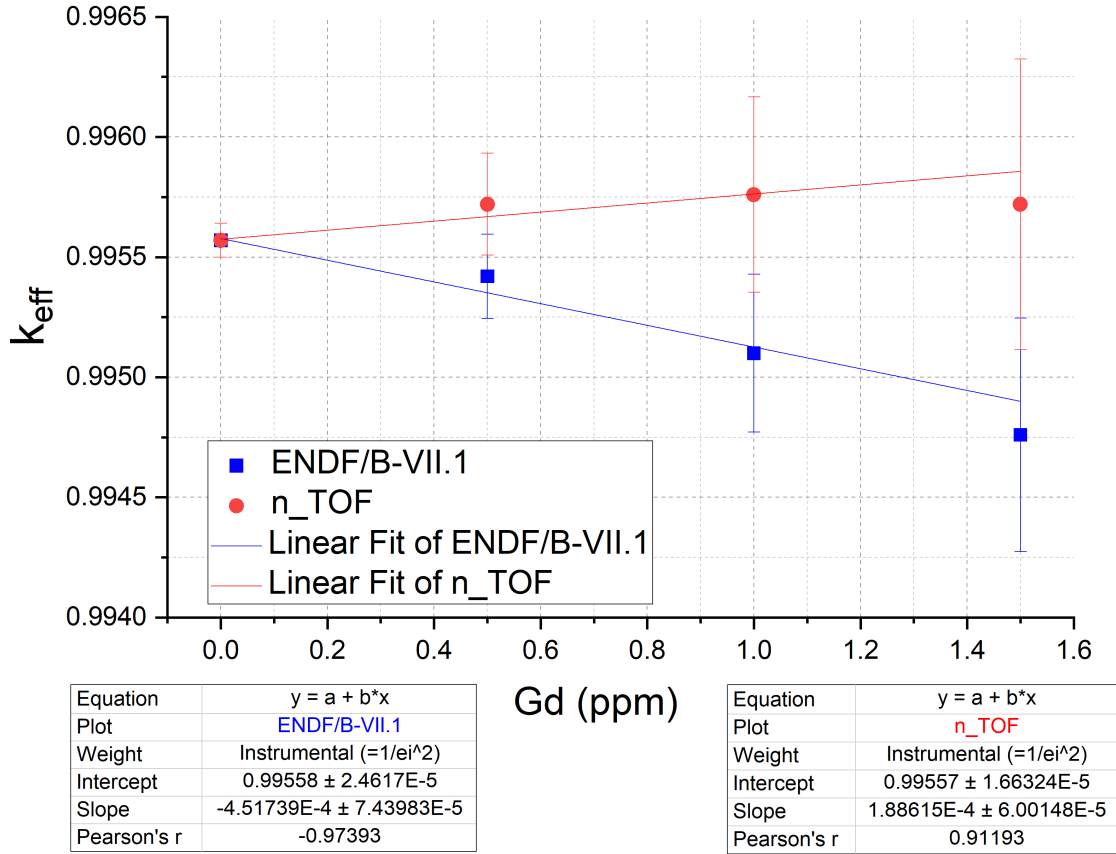


Figure 3.8:  $k_{eff}$  multiplication factor comparison in cases G1, G2, G3, G4 for the MCNP ZED-2 reactor core model, in the case of n\_TOF elaborated Gd cross-sections data (for isotopes  $^{155}\text{Gd}$  and  $^{157}\text{Gd}$ ) and ENDF/B-VII.1 Gd cross-sections data.

The first source of uncertainty to consider is the statistical MCNP calculation uncertainty  $\sigma_{stat}$ . As reported in Table 3.5, by employing 500,000 histories per cycle and a total of 5,000 cycles (4,950 active cycles), the statistical uncertainty is very low, and for every simulation we have  $\sigma_{stat} = 0.00001 = 0.01$  mk.

The  $\sigma_{exp}$  term is due to experimental uncertainty on core parameters, such as critical height on the moderator and moderator purity. According to Chow et al. [21], we have  $\sigma_{exp} = \sqrt{\sigma_{hc}^2 + \sigma_{pur}^2} = 0.07$  mk.

The third term considered in 3.1 is the calibration uncertainty  $\sigma_{cal}$  due to the calibration procedure described in paragraph 3.3.1. We have a boron calibration uncertainty  $\sigma_{cal_B} = \sqrt{\sigma_{stat_B}^2 + \sigma_B^2} = 0.04$  mk/ppm, where  $\sigma_{stat_B}$  is the statistical uncertainty in the boron simulations (0.06 mk in the Chow et al. [21] calculations) and  $\sigma_B$  is the  $k_{eff}$  uncertainty due to boron cross-sections, which is simply the boron reactivity worth (per ppm) times by the boron relative error of  $\pm 0.1\%$  about the thermal region, yielding  $\sigma_B = 0.07$  mk, which is 0.2% of the total boron reactivity worth<sup>5</sup> of  $-33.6$  mk (with 6 ppm of nominal boron). Since we adopt the same calibration factor for gadolinium, we have  $\sigma_{cal} = \rho_{Gd} \cdot (0.2\%) = 0.04$  mk/ppm, with

<sup>5</sup> So that the complete calibration factor is  $-1.2\% \pm 0.2\%$

an estimated Gd reactivity  $\rho_{Gd} = -20.1$  mk/ppm.

The last term in Equation 3.1 is due to the uncertainty in Gd absorption cross-sections, particularly in the thermal energy range.  $\sigma_{Gd}$  is given by a sensitivity calculation, of the type of Equation 2.24. In accordance with Chow et al. [21], we may assume a  $^{157}\text{Gd}$  relative uncertainty of  $\pm 2\%$  for the ENDF/B-VII.1 cases, whereas we considered a  $3\%$  uncertainty for the n\_TOF Gd cross-sections data [25]. Hence we have  $\sigma_{Gd-ENDF/B} = 0.32$  mk/ppm and  $\sigma_{Gd-n\_TOF} = 0.48$  mk/ppm.

Note how the third and fourth term are proportional to the amount of dissolved gadolinium, hence varying from case to case. The fourth term  $\sigma_{Gd}$  is the major source of uncertainty, and in case G3 (1.0 ppm Gd) it accounts for around  $80\%$  of the total uncertainty on  $k_{eff}$ . The calculated uncertainties are reported in Tables 3.6 and 3.7 and represented graphically in Figure 3.8.

ENDF/B	$\sigma_{stat}$	$\sigma_{exp}$	$\sigma_{cal}$	$\sigma_{Gd}$	$\sigma_{k_{eff}}$
G1	0.01	0.07	0	0	0.07
G2	0.01	0.07	0.02	0.16	0.2
G3	0.01	0.07	0.04	0.32	0.4
G4	0.01	0.07	0.06	0.48	0.6

Table 3.6: Partial uncertainties on the  $k_{eff}$  values in the four cases, with gadolinium data from the ENDF/B-VII.1 library.

n_TOF	$\sigma_{stat}$	$\sigma_{exp}$	$\sigma_{cal}$	$\sigma_{Gd}$	$\sigma_{k_{eff}}$
G1	0.01	0.07	0	0	0.07
G2	0.01	0.07	0.02	0.24	0.3
G3	0.01	0.07	0.04	0.48	0.6
G4	0.01	0.07	0.06	0.72	0.8

Table 3.7: Partial uncertainties on the  $k_{eff}$  values in the four cases, with gadolinium data from the n\_TOF measurements.

# Conclusion

Gadolinium is used as a burnable reactor poison in many GEN-II and GEN-III nuclear power reactors. For its importance as a safety device, then, accurate knowledge of its nuclear data is required.

In this work, we examined the behaviour of the gadolinium odd isotopes in the context of criticality calculations performed via the MCNP6.2 code, with reference to the ENDF/B-VII.1 library. The benchmarks analysed are the MCNP input files developed by Chow et al. [21] for the ZED-2 research reactor, AECL, Canada. A total of 4 cases were examined, each with a different gadolinium concentration. Thanks to the great computational power offered by the CRESCO servers (ENEA) where the code was run, a large number of histories per cycle and a large number of cycles were set for each simulation. The preliminary checks showed that the criticality calculations entail an almost immediate convergence of the effective multiplication factor  $k_{eff}$ , which is close to but less than 1 for all of the four cases. Similarly, the Shannon entropy of the fission source also converges rapidly.

It was shown that the reactor models have thermal spectra, for all of the four cases. As the gadolinium concentration increases, the spectra harden, with lower thermal peaks in the cases with more dissolved gadolinium. The reactor core was shown to be sensitive to variations in the gadolinium odd isotopes cross-sections, especially to  $^{157}\text{Gd}(n,\gamma)$ . Higher gadolinium concentrations determine higher sensitivities and, in fact, around thermal, the sensitivity is almost proportional to the gadolinium concentration in the moderator.

The gadolinium data from the ENDF/B-VII.1 library also shows that a bias on  $k_{eff}$  of  $-45 \pm 7$  pcm/ppm Gd is present, with higher gadolinium concentrations determining lower-than-expected effective multiplication factor values. For the reasons listed in the initial chapter of this work, new gadolinium data were measured at n\_TOF (CERN). Criticality simulations that included the newly evaluated data were then carried out and compared to the simulations where the gadolinium ENDF/B-VII.1 data were used. With the n\_TOF data, the bias is partly corrected and reduces to  $19 \pm 6$  pcm/ppm Gd. Hence, the n\_TOF cross-sections represent an improvement in the context of ZED-2 reactor criticality simulations. The obtained cross-sections were submitted to the EXFOR database in 2019.

# Acknowledgements

I wish to thank my supervisors, Professor Cristian Massimi and Dr. Patrizio Console Camprini, for their valuable help and for the vast amount of documentation they made available. I also wish to thank Dr. Manuela Frisoni for the development of the ACE-format files containing the n\_TOF campaign Gd cross-sections used for the simulations.

The computing resources and the related technical support used for this work have been provided by CRESCO/ENEAGRID High Performance Computing infrastructure and its staff [23]. CRESCO/ENEAGRID High Performance Computing infrastructure is funded by ENEA, the Italian National Agency for New Technologies, Energy and Sustainable Economic Development and by Italian and European research programmes.

# Acronyms and Abbreviations

ACE	A Compact ENDF
AECL	Atomic Energy of Canada Limited
BOL	Beginning of life
C/E	Calculated/Experimental
CANDU	Canada Deuterium Uranium
CERN	European Organisation for Nuclear Research
CRESCO	Computational RESearch Centre on COMplex systems
CTBTO	Comprehensive Nuclear-Test-Ban Treaty Organisation
DR	Dominance Ratio
EAR	Experimental Area
ENDF	Evaluated Nuclear Data File
ENEA	Italian National Agency for New Technologies, Energy and Sustainable Economic Development
EPR	European Power Reactor
FA	Fuel assembly
fBIF	Beam Interception Factor
Hsrc	Source entropy (Shannon entropy)
IAEA	International Atomic Energy Agency
ICSBEP	International Criticality Safety Benchmark Evaluation Project
INFN	National Institute for Nuclear Physics
IRPhEP	International Reactor Physics Experiment Evaluation Project
JANIS	Java-based nuclear information software
JEFF	Joint Evaluated Fission and Fusion Nuclear Data Library
JENDL	Japanese Evaluated Neutron Data Library
Keff	Effective multiplication factor
LWR	Light water reactor
MCNP	Monte Carlo N-Particle
n_TOF	Neutron Time of Flight
NEA	Nuclear Energy Agency
NIDC	National Isotope Development Center
OECD	Organisation for Economic Co-operation and Development
ORNL	Oak Ridge National Laboratories
PHWT	Pulse Height Weighting Technique
PWR	Pressurised water reactor

## *APPENDIX A. ACRONYMS AND ABBREVIATIONS*

---

SFP	Spent fuel pool
XS	Cross section
ZED-2	Zero Energy Deuterium reactor

# Bibliography

- [1] International Atomic Energy Agency (IAEA). *The Statute of the IAEA*. URL: <https://www.iaea.org/about/statute>.
- [2] E. E. Lewis. *Fundamentals of Nuclear Reactor Physics*. Academic Press, 2008, pp. 255, 256. DOI: <https://doi.org/10.1016/B978-0-12-370631-7.X0001-0>.
- [3] F. Rocchi et al. “Reassessment of gadolinium odd isotopes neutron cross sections: scientific motivations and sensitivity-uncertainty analysis on LWR fuel assembly criticality calculations”. In: *EPJ Nuclear Sci. Technol.* 3 (2017), p. 21. DOI: 10.1051/epjn/2017015.
- [4] E. E. Lewis. *Fundamentals of Nuclear Reactor Physics*. Academic Press, 2008, p. 40. DOI: <https://doi.org/10.1016/B978-0-12-370631-7.X0001-0>.
- [5] G. Leinweber et al. “Neutron Capture and Total Cross-Section Measurements and Resonance Parameters of Gadolinium”. In: *Nuclear Science and Engineering* 154.3 (2006), pp. 261–279. DOI: 10.13182/NSE05-64.
- [6] M. B. Chadwick et al. “ENDF/B-VII.1 Nuclear Data for Science and Technology: Cross Sections, Covariances, Fission Product Yields and Decay Data”. In: *Nuclear Data Sheets* 112.12 (2011), pp. 2887–2996. ISSN: 0090-3752. DOI: <https://doi.org/10.1016/j.nds.2011.11.002>.
- [7] S. F. Mughabghab. *Atlas of Neutron Resonances: Volume 2: Resonance Properties and Thermal Cross Sections Z= 61-102*. Elsevier, 2018, p. 168.
- [8] D. Bernard and A. Santamarina. “Qualification of gadolinium burnable poison: Interpretation of MELUSINE/GEDEON-II spent fuel analysis”. In: *Annals of Nuclear Energy* 87 (2016), pp. 21–33. ISSN: 0306-4549. DOI: <https://doi.org/10.1016/j.anucene.2015.02.034>.
- [9] S. C. van der Marck. “Benchmarking ENDF/B-VII.1, JENDL-4.0 and JEFF-3.1.1 with MCNP6”. In: *Nuclear Data Sheets* 113.12 (2012), pp. 2935–3005. ISSN: 0090-3752. DOI: <https://doi.org/10.1016/j.nds.2012.11.003>.
- [10] J. D. Bess et al. “The 2019 Edition of the ICSBEP Handbook”. In: (Nov. 2019). URL: <https://www.osti.gov/biblio/1634112>.
- [11] N. Soppera, M. Bossant, and E. Dupont. “JANIS 4: An Improved Version of the NEA Java-based Nuclear Data Information System”. In: *Nuclear Data Sheets* 120 (2014), pp. 294–296. ISSN: 0090-3752. DOI: <https://doi.org/10.1016/j.nds.2014.07.071>.

- [12] CERN. *n\_TOF The neutron time-of-flight facility at CERN*. URL: <https://ntof-exp.web.cern.ch/>.
- [13] C. Guerrero et al. “Performance of the neutron time-of-flight facility n\_TOF at CERN”. In: *The European Physical Journal A* 49.2 (Feb. 2013), p. 27. ISSN: 1434-601X. DOI: 10.1140/epja/i2013-13027-6.
- [14] M. Mastromarco et al. “Cross section measurements of  $^{155,157}\text{Gd}$  ( $n,\gamma$ ) induced by thermal and epithermal neutrons”. In: *The European Physical Journal A* 55.1 (2019), pp. 1–20.
- [15] F. Rocchi and D. M. Castelluccio. “Implementation of a cross section evaluation methodology for safety margins analysis: techniques and experimental campaign for new evaluations of neutron capture cross sections of Gadolinium odd isotopes”. In: (2017).
- [16] F. B. Brown. “Fundamentals of Monte Carlo particle transport”. In: *Los Alamos National Laboratory, LA-UR-05-4983* (2005).
- [17] X\_5 Monte Carlo Team et al. *MCNP A General Monte Carlo N-Particle Transport Code Version 5 Volume I: Overview and Theory*. 2003.
- [18] F. B. Brown. “On the use of Shannon entropy of the fission distribution for assessing convergence of Monte Carlo criticality calculations”. In: (2006).
- [19] C. J. Werner (editor). *MCNP User’s manual code version 6.2. Los Alamos (NM): Los Alamos National Laboratory*. report LA-UR-17-29981 (2017).
- [20] J. E. Atfield. “28-element natural UO<sub>2</sub> fuel assemblies in ZED-2”, ZED2 HWR EXP 001”. In: *International Handbook of Evaluated Reactor Physics Benchmark Experiments–IRPhEP* (2006).
- [21] J. C. Chow et al. “Nuclear Data and the Effect of Gadolinium in the Moderator”. In: *AECL Nuclear Review* 1.1 (2012), pp. 21–25. DOI: 10.12943/ANR.2012.00004.
- [22] CNL. *ZED-2 Research Reactor*. URL: [https://www.cnl.ca/site/media/Parent/ZED-2\\_Eng.pdf](https://www.cnl.ca/site/media/Parent/ZED-2_Eng.pdf).
- [23] F. Iannone et al. “CRESCO ENEA HPC clusters: a working example of a multifabric GPFS Spectrum Scale layout”. In: *2019 International Conference on High Performance Computing Simulation (HPCS)*. 2019, pp. 1051–1052.
- [24] P. Console Camprini et al. “PAR2018-ADPFISS-LP1-129”. In: (Jan. 2019). DOI: 10.13140/RG.2.2.24916.24963.
- [25] F. Rocchi et al. “Sensitivity uncertainty analysis and new neutron capture cross-sections for gadolinium odd-isotopes to support nuclear safety”. In: *Annals of Nuclear Energy* 132 (2019), pp. 537–543.